Copper-independent lysosomal localization of the Wilson disease protein ATP7B

Saptarshi Maji, Ruturaj, Tamal Ghosh, Santanu Das[$], Arnab Gupta*

Department of Biological Sciences, Indian Institute of Science Education and Research Kolkata, Mohanpur, West Bengal -741246, India

[$]Present address: Children's Hospital of Philadelphia and University of Pennsylvania, Philadelphia, PA 19104

*Correspondence to: arnab.gupta@iiserkol.ac.in

Running title: ATP7B constitutively localize on lysosomes

Synopsis: Excess copper is toxic to the cell. In Hepatocytes, the Wilson disease protein, ATP7B has been reported to recycle between the trans-Golgi network and lysosomes to export copper in elevated copper condition. We for the first time show that a large fraction of ATP7B constitutively reside on the lysosome and rather the position of the lysosome shifts from TGN-proximal to peripheral region of the cell in high copper to facilitate ATP7B-mediated lysosomal exocytosis of copper.

The authors declare no competing financial interests.

Abstract

In hepatocytes, the Wilson disease protein, ATP7B resides on trans-Golgi network and traffics to peripheral lysosomes to export excess intracellular copper by means of lysosomal exocytosis. We found that in basal copper or even upon copper chelation, a significant amount of ATP7B persists on endolysosomal compartment of hepatocytes but not in non-hepatic cells. These ATP7B-harboring lysosomes lie in close proximity of < 40 nm to the TGN. ATP7B constitutively distributes itself between the the sub-domain of the TGN with a lower pH and the TGN-proximal lysosomal compartments. Localization of ATP7B on TGN-Lysosome hybrid compartments upon Golgi disruption suggested possible exchange of ATP7B directly between the TGN and its proximal lysosomes. Manipulating lysosomal positioning significantly alters the localization of ATP7B in the cell. Contrary to previous understanding, we found that upon copper chelation in a copper replete hepatocyte, ATP7B is not retrieved back to TGN from peripheral lysosomes; rather ATP7B recycles to these TGN-proximal lysosomes to initiate the next cycle of copper transport. We report a hitherto unknown copper-independent localization of ATP7B i.e., at the lysosomes and also the importance of TGN-proximal lysosomes but not TGN as the terminal acceptor organelle of ATP7B in its retrograde pathway.

Keywords: ATP7B, Wilson disease, hepatocytes, endolysosomes, Trans-Golgi Network, TGN-proximal lysosomes

Introduction

Wilson disease (WD) is caused due to mutations in the copper transporting ATPase leading to copper accumulation in the liver (Gupta et al., 2018; Lutsenko et al., 2008; Gupta and Lutsenko, 2009; Bull et al., 1993; Petrukhin et al., 1994). Lysosomal exocytosis serves as a key process in order to maintain optimal intracellular levels of the physiologically crucial micronutrient, copper (Polishchuk et al., 2014; Peña et al., 2015; Polishchuk and Polishchuk, 2016; Das et al., 2020). Lysosome is the primary organelle that serves as the regulatory hub for recycling and homeostasis in a cell. Being a dynamic organelle, it interacts with other organelles and endosomal system to maintain a multitude of crucial homeostatic functions (Lim and Zoncu, 2016; Mony et al., 2016; Ballabio and Bonifacino, 2020). Variety of cellular signalling can affect lysosomal size, number, and position rapidly. Distribution of lysosomes in terms of its size, position, acidity and number are important indicator of lysosomal health. These factors are connected and accounts for proper functioning of lysosome. Lysosomal exocytosis is one of the many important processes that lysosome undergoes to serve several important purposes like cellular clearance, membrane repair and secretory functions. Toxic cellular disposals including pathogens, heavy metals etc. that are deposited to lysosome is cleared by this essential process and failure to this can lead to several pathological conditions (Settembre et al., 2013).

Lysosomal positioning is another important factor depicting lysosome health and is related to lysosomal exocytosis (Korolchuk et al., 2011). Depending on distance from nucleus, lysosomes can be divided into two types. Lysosomes near to nucleus are known as perinuclear lysosome. Lysosomes away from nucleus are known as peripheral lysosome (Pu et al., 2016). These two types of lysosomes are different from each other in their luminal content and are tightly regulated. mTOR is one of the important regulators of these lysosomes. mTOR activation leads to anterograde trafficking of lysosome towards plasma membrane where mTOR downregulation leads to retrograde trafficking of lysosome towards nucleus (Puertollano, 2014; Hong et al., 2017).

Copper is an important micronutrient for all eukaryotes, acting as co-factor for an array of cupro-enzymes. But copper, at elevated level is detrimental to the cell. Hence the concentration of intracellular copper is tightly regulated (Balamurugan and Schaffner, 2006). Copper is up-taken in the cell via high affinity copper transporter CTR1, where environmental Cu^{2+} is reduced to bio-available and utilizable Cu^{+} (Kar et al., 2022; Kuo et al., 2001). Subsequently, copper is sequestered by cellular copper chaperons that delivers copper to different parts of cell. Atox1 delivers copper to TGN-localized ATP7A and ATP7B, the two copper ATPases (Kaplan and Maryon, 2016). At physiological copper level, ATP7A and ATP7B pumps copper into TGN lumen that serves as a site for maturation of cuproproteins. At elevated cellular copper condition, the Cu-ATPases vesicularizes from TGN and traffics to endolysosomes to export out excess copper (La Fontaine and Mercer, 2007).

Several factors govern trafficking of ATP7B. The cytoplasmic amino-terminal sequence was found to be important for copper responsive trafficking of ATP7B (Hasan et al., 2012; Braiterman et al., 2015). WD causing mutations on conserved cytoplasmic domain of ATP7B can lead to either loss of copper-responsive trafficking from the TGN or constitutive vesicularization of the protein even in copper-limiting conditions. Engineered mutations on the trileucine motif (^{1454}LLL^{1456}) causes constitutive vesicularization of the protein (Cater et al., 2006). Similarly, S340/341A mimics copper saturated amino terminal of ATP7B leading to copper independent vesicularization (Hasan et al., 2012). On the other hand, high copper fails to trigger trafficking of ATP7B harboring the WD causing mutation S653Y (Braiterman et al., 2014). Recent studies have shown ATP7B can even traffic without the influence of copper in presence of several anti-cancer drugs (Purkait et al., 2019).

The crosstalk between lysosome and ATP7B is important for maintaining proper copper homeostasis inside cell. With increasing cellular copper levels, ATP7B traffics towards endo-lysosomal compartment to pump the excess copper into lysosomal lumen. Increase in cellular copper level downregulates mTOR activity, which in turn activates TFEB and lysosomal biogenesis is upregulated. Elevated copper also triggers lysosomal exocytosis, and thus excess copper is excreted out (Polishchuk et al., 2014; Peña et al., 2015; Peña and Kiselyov, 2015).

In this study, we have shown that a significant amount of ATP7B is present on the endo-lysosomal compartment irrespective of cellular copper concentration and this localization of ATP7B is exclusively hepatocyte specific. We further observed a pool of lysosomes apposing close to the TGN that harbours this fraction of lysosomal ATP7B in basal or copper chelated condition. We also found that lysosomal positioning influences localisation of ATP7B at these TGN-proximal lysosomes. Finally, we have demonstrated that the recycling of ATP7B by the retrograde pathway that is triggered by copper chelation in copper replete cells, terminates at TGN-proximal lysosomes in contradiction to TGN as the terminal location as previously reported.

Results

ATP7B localizes on endolysosomes independent of intracellular copper concentration

The Wilson disease protein, ATP7B is sole regulator of physiological copper levels in the mammalian liver. ATP7B is primarily expressed in hepatocytes (Fanni et al., 2005), though its expression in non-hepatic tissues is also reported (Barnes et al., 2009; Michalczyk et al., 2008; Peña et al., 2015). It is well documented that ATP7B under basal intracellular conditions localizes at the trans-Golgi network (TGN) and helps in transporting copper to the TGN lumen which is being utilized by various copper dependent proteins (Polishchuk and Lutsenko, 2013). In hepatocytes, at elevated intracellular copper ATP7B traffics to the endolysosomal compartment for exporting copper from cytosol which is subsequently excreted out of the cell via copper-induced increased lysosomal exocytosis (Gupta and Lutsenko, 2009; Gupta et al., 2018; Lutsenko, 2016). Upon removal of copper by chelators, ATP7B has been reported to recycle back to the TGN (Polishchuk and Polishchuk, 2019).

We determined localization of ATP7B in HepG2 cells in basal and elevated copper conditions. Interestingly, to our surprise at basal copper (cells not treated with extracellular copper), a significant amount of ATP7B constitutively localized at the endolysosomal compartment as determined its colocalization with the lysosomal marker LAMP2 (Fig 1A). We found that 56.4±21% (mean±SD) of total ATP7B localizes at the endolysosomal compartments in basal conditions. As expected, upon copper treatment (20, 100 and 250µM), the fraction of ATP7B in the TGN decreases coupled with its increased colocalization with LAMP2 (Fig 1B, S1A, S1B). We found a similar trend in case of LAMP1 as endolysosomal marker (fig S2). When copper was chelated from the cell using cell-impermeable copper chelator BCS (Bathocuproinedisulfonic acid) or cell permeable chelator TTM (Tetrathiomolybdate), the endolysosomal localization of ATP7B decreases but do not entirely disappear (Fig 1A). Interestingly, the combined fraction of ATP7B present in TGN and endolysosomal compartment remains unchanged irrespective of copper treatment supporting the idea of ATP7B recycling exclusively between these two compartments (Fig 1C). Changes of intracellular copper concentration with increasing copper treatment in the treatment media was confirmed by ICP-OES measurement of cellular copper concentration (Fig 1D). Total abundance of the ATP7B protein did not change significantly with varying copper levels in the treatment media, though a slight increase was observed for cell treated with 100µM and 250µM copper (Fig 1E).

To substantiate our finding on distribution of ATP7B in lysosome vs TGN, we employed sub-cellular fractionation, to isolate 13 fractions of cellular lysate and identified different Golgi and endolysosome rich fractions. Presence of ATP7B in both compartments at basal condition were confirmed by immunoblot (Fig 1F). Since, hepatocytes deploy lysosomal exocytosis to export excess copper out of the cell, we found our observation of ATP7B localizing in lysosomal compartments even in basal and copper chelated conditions thought provoking that demanded further investigation.

Endolysomal localization of ATP7B in basal copper condition is hepatocyte-specific

We further investigated whether this property of ATP7B localizing at endolysosomal compartments in low and limiting copper is a ‘cell-type’ specific phenomenon or is observed globally. In Huh7, another hepatic cell line derived from hepatoma tissue, we found a similar localization pattern of ATP7B (Fig 2A, 2B). Levels of copper did not significantly influence the abundance of total ATP7B in these cells as observed earlier in HepG2 (Fig. 2C). To further examine our findings in non-hepatic cells, we proceeded in HeLa and kidney cell line HEK293T. Presence of ATP7B in other cell lines were confirmed by immunoblotting and compared with hepatic cell lines, HepG2 and Huh7 (Fig 2D). Interestingly, both in HeLa and HEK293T, the endogenous ATP7B were present in only TGN in basal copper condition. No endolysosomal localisation was observed in basal copper condition. As observed in hepatocytes, in elevated copper condition, ATP7B traffics from TGN to endolysosomal compartment in HeLa that was determined by diminished colocalization of ATP7B with TGN46 and increasing colocalization

with LAMP2 (Fig 2E, 2F). In HEK293T cells, as previously reported, minimal TGN exit of ATP7B was observed in high copper condition as determined by colocalization between ATP7B, LAMP2 and TGN markers, TGN46 (Fig S3A). To examine if the difference in ATP7B localization may be due to underlying sequence differences of the cDNA between hepatic and non-hepatic cells, we ectopically expressed mEGFP-ATP7B (cloned from liver cDNA) in HeLa. The protein did not exhibit any endolysosomal localization at basal or copper-limiting condition. At elevated copper concentration, mEGFP-ATP7B was found to be exiting TGN and localizing at the endolysosomal compartment which confirms copper responsive trafficking of ATP7B in non-hepatic cell lines (Fig S3B)

We tested if the localization pattern of ATP7B in hepatocytes is reproduced by its homologue copper ATPase, ATP7A (Menkes disease protein). Interestingly, under basal condition, ATP7B exhibits a higher vesicular localization as compared to ATP7A (Fig 2G *top panel*). Unlike ATP7B, ectopically expressed ATP7A (mKO-ATP7A) in HepG2 did not localize at the endolysosomal compartments marked by LAMP2 (Fig 2G *bottom panel*), though it exhibited copper responsive exit from the TGN in high copper (Fig S3C). From these experiments, we conclude that copper independent endo-lysosomal localisation is a specialized feature of ATP7B when expressed exclusively in hepatic cell lines.

ATP7B recycles between TGN-proximal lysosomes and the TGN in a copper-independent mode

Upon close examination, we found that the TGN and lysosomes are in close proximity in multiple locations in the perinuclear region of the cell and even these two structures may possibly share some contact sites. Interestingly, we found out that an appreciable fraction of ATP7B is localised on these TGN-proximal lysosomes. We observed similar localisation pattern of ATP7B using various TGN and endo-lysosomal marker combination i.e., TGN46-LAMP2 (Fig 3A), TGN46-LAMP1 (Fig S4A), Golgin97-LAMP1 (Fig S4B) and TGN38-LAMP2 (fig S4C). ATP7B localizing at TGN46 and late endosome marker Rab7 was significantly diminished as compared to the *bona fide* lysosomal markers (Fig S4D). Not only in HepG2, but we observed similar phenomenon for another hepatic cell line Huh7 (Fig S4E). We calculated that under basal copper condition a fraction of ATP7B (5.3±4%, mean±SD) was present where TGN marker TGN46 and endo-lysosomal maker LAMP2 colocalizes.

To obtain a higher spatial resolution, we utilised stimulated emission depletion (STED) microscopy to look further into ATP7B distribution at the TGN and the TGN-proximal lysosomes. Our inference of ATP7B localisation in TGN-proximal lysosomes stayed valid (fig 3B) irrespective of cellular copper condition.

We utilized proximity ligation assay (PLA) to further substantiate our finding that TGN and these TGN-proximal lysosomes constitutively harboring ATP7B (copper-independent) shares close apposition. In PLA, if two used proteins labelled by their respective antibodies are within the proximity range of 40nM with each other, a spot fluorescent emission is detected through in-cell PCR (Söderberg et al., 2006). We labelled endolysosomes with

LAMP2 antibody and TGN with antibody against GCC2. We detected several fluorescent spots when these two antibodies were simultaneously employed. Furthermore, we found some of the PLA signal overlapped with ectopically expressed EGFP-ATP7B (fig 3C). We used ATP7B and VPS35 as the positive control as these two proteins exhibit spatial interaction as shown earlier by our group (Das et al., 2020). No PLA signal was observed in the negative controls (fig S4F). Overlap of PLA (red) signal with ATP7B (green) confirmed the presence of ATP7B on TGN-proximal lysosomes.

LAMP2 is a heavily glycosylated recycling protein that is also detected at the trans-Golgi network in the late secretory pathway (Pols et al., 2013, 41). To inspect if the TGN-lysosomal overlap is formed by TGN-localised or TGN-exiting LAMP2 in the late secretory pathway or this lysosome is a part of the maturing endocytic pathway, we performed a dextran uptake assay. Dextran is up taken by cell via endocytosis and then localises to acidic compartment by the process of endosomal maturation. Therefore, any overlap between TGN and Dextran can be accepted as a true TGN-lysosome proximity site. We found overlap between TGN marker S-galactosyl transferase and acidic compartment (dextran positive) and ATP7B was present at the overlap region in basal copper condition (fig 4A). Hence, we can confirm that a fraction of ATP7B constitutively localizes at those TGN-lysosome proximity region.

Lysosomes are dynamic organelle which is known to make contact sites with different other organelles (Hao et al., 2017; Cisneros et al., 2022; Chu et al., 2015; Lim et al., 2019). These organelles contact sites provides unique environment inside cell, important for crucial physiological functions of these organelles and inter-luminal exchanges. Hao et al. has shown that lysosome makes contacts with cis-Golgi forming unique Golgi-Lysosome contact sites (GLCS) that is important for mTOR activation in cell (Hao et al., 2017). We investigated if GLCS resides at the same zone where TGN-lysosomes share high proximity. Interestingly, we have found that GLCS formed by cis-Golgi marker GM130 and endolysosomal marker LAMP1 unique and are quite different from TGN46-LAMP1 colocalising point (Fig 4B). Moreover, ATP7B was not present in GLCS (Fig 4C). Interestingly, though TGN46 colocalises with both the endolysosomal marker LAMP1 and LAMP2 at the TGN-proximal lysosomes, the colocalisation sites between TGN46 and LAMP1 was found to be more abundant than the same between LAMP2 (Fig S5A).

We argued that if TGN and endolysosomes share high proximity and ATP7B is constitutively exchanged between these two organelles, then disrupting the Golgi should lead to formation of hybrid compartments that should have a share of both endolysosomal as well as TGN membrane. Interestingly, we observed that disrupting the Golgi using Brefeldin-A resulted in formation of punctate compartments that was positive for both LAMP2 as well as TGN46 (fig 4D, Fig S4G). Interestingly, ATP7B was found in a hybrid domain of TGN-endolysosome upon Golgi disruption. Though not appreciable, we observed a slight shift towards ATP7B-LAMP2 colocalization over ATP7B-TGN46 in BFA treated cells as compared to untreated controls (fig 4E). The post-BFA treated hybrid

compartments exhibited high ATP7B localization as compared to its presence on the TGN-proximal lysosomes (Fig S5B). The formation of a hybrid compartment carrying both TGN and lysosome membrane markers suggest the presence of a possibly direct and constitutive ATP7B-containing membrane exchange phenomenon between the two organelles.

ATP7B localizes at the region of the trans-Golgi network that exhibits lower pH

TGN and the proximal lysosomes constitutively exchange ATP7B. The TGN and lysosomes has drastically different pH, lysosomal lumen being more acidic as compared to lumen of Golgi stacks. A large amount of the ATP7B was found to be present in a milieu around the TGN and the proximal lysosomes (0.5-1.5µm). Copper ATPases are known to require slightly acidic environment for its efficient copper pumping activity (Lutsenko et al., 2007; Barry et al., 2011). Since copper pumping activity of ATP7B is pH dependent, we wanted to check if ATP7B is preferentially present in any subdomains of TGN based on pH. We used pH-sensitive pHluorin tag attached to the C-terminal of TGN38 which anchors it to the TGN membrane. The sensor, pHluorin is a modified GFP that has two pH-dependent excitations. At neutral pH, it is excitable at 395nm where at acidic pH, it gets excited at 480nm. With decreasing pH, the emission at 480nm increase as well as ratio of the two emissions Em_{480}/Em_{395} (Miesenböck et al., 1998). So, from two excitations, we can gather a qualitative idea of the luminal pH gradient (if any) and correlated preferential localization of ATP7B within the TGN. Upon expressing the pHluorin plasmid in HepG2 cells, we found that ATP7B is preferentially present on the acidic sub-domain of TGN as visualized by its higher colocalization with pHluorin when excited by the wavelength of 480nm as compared to excitation at 395nm (fig 4F). We also observed that the acidic subdomain of TGN shares close proximity with lysosomes marked by dextran (Fig 4F). We can infer that the low pH organellar subdomains possibly act as the sites of direct exchange of ATP7B between the TGN and TGN-proximal lysosomes.

TGN-proximal lysosomes serve as a hub for endo-lysosomal sorting of ATP7B

ATP7B traffics to vesicles from TGN upon elevated intracellular copper levels. However, the exact mechanism of copper-induced Golgi exit mechanism for ATP7B is not well understood. It is well documented that ATP7B is directly transported to endo-lysosomal compartment (late secretory pathway), not by endocytic pathway of lysosomal maturation via plasma membrane (Polishchuk et al., 2014). To circumvent copper-induced toxicity, this type of direct transport ensures faster response in elevated copper condition. A recent study has shown that TGN associated lysosome acts as a hub for secretory, endosomal and autophagic route in drosophila (Zhou et al., 2023). Interestingly, we found that increase in TGN46-LAMP2 colocalisation is positively correlated with copper-induced endolysosomal localisation of ATP7B that increases with increasing copper (fig 5A, 5B). We further explored if these TGN-proximal lysosomes serve as a '*distribution hub'* to endolysosomal distribution

(trafficking) of ATP7B in elevated copper. First, we conducted time-lapse imaging of ATP7B trafficking during copper treated condition. Interestingly, we have found that dextran positive acidic compartments to be reaching in contact with the TGN upon 100µM copper treatment. ATP7B signal was found to increasing in the dextran positive compartment and simultaneously decreasing at the TGN which suggests possible ATP7B exchange between these two compartments (fig 5C, Video 1). These findings reveals that high copper induces localization of endolysosomal compartments at the TGN where ATP7B exchange occurs between the TGN (donor compartment) and the lysosomes (acceptor compartment).

Since no modulator for TGN-proximal lysosomes is yet known, we employed indirect methods to manipulate ATP7B localisation at these sites. More than 400 WD causing mutations are known for the ATP7B protein. Many of them results in defective trafficking of the protein (Das et al., 2022). H1069Q, the most prevalent mutations reported in Caucasian population exhibits compromised copper-induced Golgi exit of the protein (Payne et al., 1998). Another WD mutation S653Y though capable of copper transport at the Golgi, shows complete non-trafficking phenotype (Braiterman et al., 2014). We tested if these mutants differ as compared to the wt ATP7B with respect to their presence on the TGN-proximal lysosomes. Upon expressing EGFP-tagged mutant ATP7B and the wt ATP7B, we found that Golgi retained mutants (H1069Q and S653Y) show much reduced TGN-proximal lysosome localisation than wildtype ATP7B (fig 5D). This observation indicates that 'trafficking-ready' ATP7B resides at these TGN-proximal vesicles that possibly serves as the exit point for copper-induced trafficking.

Lysosomal positioning regulates ATP7B abundance at the TGN-proximal lysosomes

Lysosomal positioning is one of the major indicators of cellular health. Depending upon nutrient status of the cell, lysosomes could be either attain perinuclear or peripheral localization in a mammalian cell (Pu et al., 2016; Korolchuk et al., 2011; de Martín Garrido and Aylett, 2020; Oyarzún et al., 2019). In addition to that, endolysosomes that are at the proximity to TGN are essentially perinuclear lysosome. So, we wanted to ask if lysosomal positioning at these TGN-proximal sites or at the cell periphery have any effect on localisation of ATP7B. We overexpressed lysosomal position-modulating proteins to enrich either perinuclear or peripheral lysosomes.

RUFY3 is an important modulator for retrograde trafficking of lysosome. It is a member of a small group of proteins called RUFY or "RUN and FYVE domain-containing protein" that acts as adaptor to small G-proteins specifically (Char and Pierre, 2020). RUFY3 is an effector of Arl8b that promotes the formation JIP4-dynein-dynactin complex and thus modulates retrograde trafficking of Lysosome. Overexpressing RUFY3 promotes perinuclear localisation of lysosome (Kumar et al., 2022). On the other hand, overexpressing Arl8b results in increased lysosomal localisation towards cell periphery. Arl8b is an Arf-like small GTPase that plays a crucial

role in regulating lysosomal positioning. Like other GTPases, upon GTP bound condition, the active form of Arl8b localises on lysosomes and promotes anterograde trafficking of lysosome towards periphery (Keren-Kaplan and Bonifacino, 2021; Khatter et al., 2015; Marwaha et al., 2017; Johnson et al., 2016; Kumar et al., 2022). In Arl8b overexpressed cell, we did not observe any change in endolysosomal localisation of ATP7B (fig 6A (i), (ii). However, there was a significant decrease in the abundance of TGN-proximal lysosomesas determined by calculating the signal overlap between LAMP2 and TGN46 (Fig 6A (iii)). In cells overexpressing RUFY3, we observed increased endo-lysosomal localisation of ATP7B and decreased TGN localisation than un-transfected cells (control) at basal condition (fig 6A (iv), (v). However, though we observed only a slight increase in TGN-proximal lysosomes, the difference was non-significant (fig 6A vi). In summary, increasing perinuclear lysosomal fraction shifted ATP7B pool towards endolysosomal compartment in basal condition. Facilitated exchange of ATP7B between TGN and perinuclear lysosomes (as compared to TGN-peripheral lysosomes) could be the underlying reason towards this observation. Cells overexpressing Arl8b and RUFY3 (pseudo colour in purple) have been shown in Fig S5C.

We further modulated mTOR to manipulate the fraction of peripheral and perinuclear lysosomes. mTOR (mammalian Target Of Rapamycin) is a serine/threonine kinase that, upon activation, is present on lysosomal membrane (Sancak et al., 2010). This protein forms complexes (mTORC1 and mTORC2) that has a huge impact on lysosomal functionality and localization that in turn affects a spectrum of cellular processes (Betz and Hall, 2013; Puertollano, 2014; Hong et al., 2017). In elevated copper condition, mTOR is known to get inhibited by some unknown mechanism (Peña and Kiselyov, 2015). Cu mediated inactivation of mTOR leads to upregulation of TFEB which in turn upregulates lysosomal biogenesis to exocytose extra copper from cell (Polishchuk et al., 2014; Peña et al., 2015). Further, inhibiting mTOR using rapamycin also results in perinuclear localisation of lysosomes. So, we wanted to create a similar Cu-stressed environment inside cell in absence of copper. Interestingly, in rapamycin treated cells, we observed elevated lysosomal localisation of ATP7B than TGN localisation irrespective of cellular copper condition (fig 6B (i), (ii)). Moreover, colocalisation between TGN46 and LAMP2 was also increased indicating an increase in TGN-proximal lysosomes (fig 6B (iii). Interestingly, copper treatment leads to increased lysosomal biogenesis which was measured by immunoblotting LAMP1 and LAMP2, though, we didn't observe any change in late endosomal marker Rab7 level (fig 6C, 6D). In addition, we also observed slight increase in lysotracker intensity labelling the lysosomes in flow cytometry analysis of cells in copper treated condition (fig 6E)

To summarize, increasing the perinuclear lysosomes augments endolysosomal localization of ATP7B that happens via exchange of the protein between the TGN and its proximal lysosomes. Also, to efficiently export excess copper from the cell by lysosomal exocytosis, the cell employs increased lysosomal biogenesis in elevated copper.

ATP7B recycles back to TGN-proximal lysosomes upon copper chelation

In elevated copper condition, ATP7B exports the excess copper via lysosomal exocytosis. Subsequently, upon copper chelation, ATP7B recycles from endolysosome in a retromer regulated pathway (Das et al., 2020). So next, we asked whether the vesicularized (trafficked) ATP7B, upon copper-chelation completely recycles back to the TGN. For studying the retrograde trafficking of ATP7B, we treated cells with 250μM of copper for 2 hrs and then chelated with 25μM of copper chelator, TTM and recorded its trafficking using time lapse imaging. Interestingly, while tracking the retrograde pathway using live imaging, we found that acidic compartments marked by dextran carrying ATP7B returns from peripheral location to perinuclear location but the endolysosomal pool of ATP7B does not relocalize to the TGN. Rather, it remained localised in acidic compartments that are juxtaposed to the TGN (fig 7A and video 2). Our observation holds true even if we continued imaging for an extended time. To avoid skewing the abundance of ATP7B in TGN pool due to *de novo* synthesis of the protein, we halted protein synthesis using cycloheximide (CHX) during the entire time period of the experiment. We found that, in cycloheximide treated condition, even after copper chelation, the TGN pool and the total endosomal pool of ATP7B remained similar as copper treated condition. Interestingly, upon triggering the retrograde pathway of ATP7B with the copper chelator BCS for 30 mins or continued for 2h, ATP7B was detected in peri-Golgi lysosomes with a fraction of it localizing at very close proximity to the TGN (shown by white arrows in Fig. 7B, bottom panel of CHX treatment, magnified insert and Fig S5D). On the contrary, in the control set (not treated with cycloheximide), the TGN localisation of ATP7B increases upon copper chelation which suggests that the TGN localised ATP7B pool is due to newly synthesized ATP7B during the entire experimental process (fig 7B, 7C, 7D). In CHX treated cells, colocalization between ATP7B and LAMP2 and the fraction of ATP7B on LAMP2- labelled endolysosomes increases with copper treatment and stays high even after activating the retrograde pathway, compared to control cells (fig 7C, S5E *top panel*). Understandably, a reverse phenomenon was observed in case of ATP7B and TGN46 colocalization and the fraction of ATP7B at the TGN46-labelled trans-Golgi network (fig 7D, S5E *bottom panel*). The comprehensive comparative analysis and box-plot of colocalization of ATP7B with LAMP2 and TGN46 between CHX treated and control cells the four copper conditions have been illustrated in Fig S5F. This finding suggests that endolysosomal fraction of ATP7B remains at the endolysosomes after activating the retrograde pathway. The retrograde pathway of ATP7B is possibly an '*incomplete recycling pathway*' ensuring that recycled ATP7B is not reinstated back to the TGN but stays in the endolysosomes closer to the peri-Golgi region of the cell. This provision might be beneficial for a quick response to elevated copper levels when ATP7B needs to conduct copper export via lysosomal exocytosis.

To set as clear cut-off distance from the nucleus that will demarcate perinuclear vs peripheral lysosomes is not possible as (a) there always exists a fraction of lysosomes that are either traveling in the anterograde or the

retrograde pathway and are yet to reach the point of final destination at the periphery or the perinucleus respectively (b) the nucleus/cell ratio is large in HepG2 cells and therefore making it difficult to clearly distinguish between the two pools of lysosomes. Since ATP7B traffics between TGN and lysosomes, it is perhaps more apt to use a Golgi centric approach instead of nuclear-centric approach for analysis of ATP7B positioning in our study. So, for the purpose of quantitation and nomenclature, we used peri-Golgi and away-from-Golgi to name two pools of ATP7B. Anything within the range of 0.5µm from the nearest TGN boundary was considered as peri-Golgi and the rest of ATP7B was pooled as away-from-Golgi (Fig 8A). This is because at basal condition most of ATP7B was found at a distance within 0.5µM from the TGN boundary. This pool of ATP7B at peri-Golgi lysosomes at four different copper conditions are depicted in Fig 8B.

To summarize our findings, in hepatocytes, ATP7B exhibits a constitutive localization in the TGN and TGN-proximal lysosomes. These post-TGN lysosomal compartments may serve as the sites where ATP7B accepts copper from ATOX1. Upon elevated copper, lysosomal trafficking from TGN-proximal to peripheral zone leads to higher vesicularization of ATP7B that can now export copper via lysosomal exocytosis. Upon copper chelation, the protein recycles back to the TGN-proximal lysosomes, but not to the TGN, to reinitiate the next round of copper transport. The present study leads us to further hypothesize that constitutive presence of ATP7B on TGN-proximal lysosomes saves the cell of energy expenditure of vesicular budding and fission from the TGN at every cycle of copper export by the Cu-ATPase.

Discussion

The Wilson disease protein, ATP7B maintains physiological levels of copper in the hepatocytes. It has been well documented that ATP7B traffics in vesicles upon copper treatment in all in vitro models of hepatocyte. At the compartments ATP7B utilizes lysosomal exocytosis to export out the excess copper (Polishchuk et al., 2014). Vesicularized ATP7B exhibits retrograde trafficking upon copper chelation. Previously we have shown that the retromer complex regulates recycling of the protein from the endolysosomal vesicles (Das et al., 2020).

In the present study we described a pool of lysosomes that lies in close proximity to the TGN and that the copper transporting ATPase, the Wilson disease protein, ATP7B localizes at these TGN-proximal lysosomes. In the last few years, organellar interfaces, e.g., ER-endosome contact sites have been shown to be modulators of multiple cellular physiology particularly, lipid transfer or recruitment of various complexes and enzymes at ER-endosome. These contact sites play an active role in endosome sorting, scission, and maturation (Lim et al., 2019; Eden, 2016; Raiborg et al., 2015; Rowland et al., 2014; Allison et al., 2017). Recently discovered Golgi-Lysosome contact sites (GLCS) has been shown to be crucial in regulating mTORC activity (Hao et al., 2017).

Why does ATP7B localize at TGN-proximal lysosomes? We found that an appreciable fraction of ATP7B is always present at these compartments. We believe that these sites act as copper dependent as well as copper-

independent TGN exit sites for ATP7B. These sites may be the initial points of the late secretory pathway for ATP7B where the ATPase pumps/transports copper even in the absence of a receptor protein e.g., Ceruloplasmin (Lutsenko et al., 2007). Our hypothesis is further supported by lower pH around these zones where these two organelles share high proximity. Lower pH acts as sites of copper release from the transmembrane domains of ATP7B that harbours the conserved copper-sequestering CPC motif as shown previously by Barry et al (Barry et al., 2011; Polishchuk et al., 2014; Gupta et al., 2018; Lutsenko et al., 2007).

We found that upon activation of the retrograde pathway, ATP7B recycles to the perinuclear zone of the cells and resides at the TGN-proximal lysosomes in contrast to its complete relocalization at the TGN, described previously (Das et al., 2020; Stewart et al., 2019, 1). We argued that recycling back from the lysosomes to the TGN is an energetically unfavourable process for the ATPase. As for each consecutive copper export cycles, ATP7B need to bud out in vesicles from the TGN, with subsequent maturation of the vesicles from early secretory vesicles to mature lysosomes where ATP7B will export copper in its lumen. To induce the retrograde trafficking pathway of ATP7B, we depleted cellular copper using extracellular copper chelator, BCS as well as intracellular copper chelator, TTM. Corroborating with our apprehensions, we found that ATP7B recycles back not to the TGN but in lysosomes that localize at close apposition with the TGN. Further, these lysosomes possibly share contact sites with the TGN. To understand the dynamics of ATP7B at the TGN-proximal lysosomes, we manipulated the lysosomal localization directly by overexpressing proteins that either triggers lysosomal trafficking from the perinuclear zone to the cell periphery or *vice versa*. Upon increasing the abundance of TGN-proximal lysosomes, we found a higher colocalization coefficient of ATP7B and LAMP2. This points towards the possible copper-independent '*anterograde movement*' of ATP7B from TGN to endolysosomes via these compartments. Elevated copper not only facilitates this process but also triggers lysosomal biogenesis to efficiently export copper and releases the cell of the copper overload.

We found that in cells of hepatic origin, ATP7B localizes at endolysosomes besides TGN in basal (physiological) as well as in depleted copper conditions. Interestingly, in hepatic cells but not in other cells of non-hepatic origin. Besides, knocking down ATP7B in HepG2 led to an adverse effect on lysosomal functioning (Polishchuk et al., 2019). In chordates, liver is the main site of nutrient recycling. Copper being a micronutrient is possibly reutilized in the cytosol and other organelles via lysosomal recycling. We hypothesize that in basal physiological conditions, endolysosome-resident ATP7B imports copper in the endolysosomal lumen upon being laden with copper by cytosol localized metallochaperone ATOX1. The less studied copper transporter of the CTR family, CTR2, might be a partner in endolysosomal copper recycling, as it has been shown to export endosomal luminal copper to the cytoplasm. ATP7B and CTR2 works in unison maintain the copper levels in the endolysosome-cytoplasm system. It has been recently shown that the S29L mutation in CTR2 has a relative higher frequency in a cohort of WD patients from China as compared to control individuals (Zhou et al., 2022). Interestingly, S29L leads to increased

intracellular Cu concentration and Cu-induced apoptosis in cultured cell lines. It would be important to further characterize the functional interplay of ATP7B and CTR2 to understand the underlying reason to localization of ATP7B at the endolysosomal compartments. A comprehensive illustration of recycling of ATP7B that summarizes our study is shown in Fig8C.

Materials and methods

Plasmids and antibodies

mEGFP-ATP7B and mKO-ATP7A constructs was available in lab. mKO-ATP7B construct was prepared by cloning ATP7B in mKO-ATP7A construct using MluI and NotI restriction site. The GFP-Arl8b and GFP-RUFY3 constructs were a kind gift from Dr. Amit Tuli, CSIR – Institute of Microbial Technology, India. Ratiometric pHluorin tagged TGN38 C-terminal and dsRed-GalT4 were a kind gift from Prof. Carolyn Machamer, Johns Hopkins University. Mutations on mEGFP-ATP7B were prepared following Q5® Site-Directed Mutagenesis Kit (NEB #E0554) protocol. Preparation of H1069Q mutant is described in Das et al (Das et al., 2022). Primers used for S653Y mutant are forward- 5'TGGAAGAAGTATTTCCTGTGC3' and reverse- 5'CTGCTTTATTTCCATCTTG3'. Plasmid isolation was done using Macherey Nuggel plasmid isolation kit (#MN740490).

Cell lines and cell culture

HepG2 cells were grown and maintained in complete medium containing low glucose Minimum Essential Medium (MEM) (Himedia #AL047S) supplemented with 10% Fetal Bovine Serum (Gibco #10270-106), 1X Penicillin-Streptomycin (Gibco #15140-122). Similarly, HEK293Tcells were grown and maintained in Dulbecco's modified Eagle's medium (DMEM) (Sigma #D6429) supplemented with 10% Fetal Bovine Serum, 1X Penicillin-Streptomycin. For transfection, JetPRIME transfection reagent (Polyplus #114-07) was used as per manufacturer's protocol.

For copper treatment, 100µM $CuCl_2$ was used for 2hrs, else mentioned otherwise. For creating copper deprived condition, cells were treated with 100 µM BCS or 25 µM TTM for 2 hrs. For small molecule treatments, Brefeldin-A (Sigma #B5936), Rapamycin (Sigma #R8781), Cycloheximide (Merck#239763) was used 30min prior to any copper treatment.

Immunofluorescence and microscopy

For fixed cell imaging, cells were fixed in 2% PFA in PBS solution for 20 min followed by PFA quenching in 50mM NH_4Cl solution for 20 min. Blocking was done in 3% BSA (bovine serum albumin) in PBSS (0.075% saponin in PBS). Cells were incubated in primary antibody in room temperature for 1.5 hrs and in secondary antibody for 30 min. After subsequent washing with PBSS, Coverslips were fixed on glass slides using SIGMA Fluoroshield™ with DAPI mountant. (Sigma#F6057) or ProLong® Gold Antifade Reagent (CST#9071). The solvent for antibody dilution was 1% BSA in PBS. For live cell imaging, cells were seeded on confocal dishes. During imaging cells were kept in imaging media containing phenol red free low glucose Minimum Essential

Medium (MEM) (Gibco #41500-034) supplemented with 10% FBS, 20mM HEPES and 1% Trolox (Sigma #238813). All images were acquired with Leica SP8 confocal platform using oil immersion 63X objective (NA 1.4) and deconvoluted using Leica Lightning software.

Details of Antibodies used are as follows: ATP7B(Abcam#124973, 1:400), TGN46 (Bio-Rad#AHP500G, 1:400), LAMP2 (DSHB#H4A3, 1:200), LAMP1 (DSHB#H4B4, 1:200; Affinity Biosciences#DF4806, 1:400), Golgin-97 (CST#13192, 1:400), Rab7a (SCBT#sc376362, 1:50), GCC2 (Atlas antibodies#HPA035849, 1:400), GM130 (BD Biosciences#610822, 1:400), TGN38 (NovusNBP103-495, 1:100), Goat anti-Rabbit Alexa488 (Thermo #A-11034, 1:2000), Goat anti-Rabbit Alexa568 (Thermo #A-11011, 1:2000), Donkey anti-Mouse Alexa 555 (Thermo #A-32773, 1:2000), Donkey Anti-Mouse Alexa405 (Abcam#ab175658, 1:1000), Donkey anti-Sheep Alexa 647 (Thermo #A-21448, 1:2000).

Immunoblotting

After respective treatment, cells were pelleted down and pellete was dissolved in 100µL of RIPA lysis buffer (10mM Tris-Cl pH 8.0, 1mM EDTA, 0.5mM EGTA, 1.0% Triton X-100, 0.1% sodium deoxycholate, 0.1% SDS, 140mM NaCl, 1X protease inhibitor cocktail, 1mM phenylmethylsulfonyl fluoride (PMSF)) and kept for 30mins on ice. The solution is then sonicated with a probe sonicator (6 pulses, 5sec, and 100mA). Bradford was used for protein quantitation and 20 µg protein was loaded in each well. Protein sample was prepared by adding 4X NuPAGE loading buffer (Invitrogen#NP0007) to a final concentration of 1X and ran on 8% SDS PAGE. This was further followed by semi-dry transfer of proteins onto nitrocellulose membrane (Milipore #IPVH00010). After transfer, the membrane was blocked with 3% BSA in TBST (TBS with 0.1% Tween20) for 3hrs at RT with mild shaking. Primary antibody incubation was done overnight at 4°C and then washed with 1X TBST (0.01% Tween-20). HRP conjugated respective secondary incubation was done for 1.5 hrs at RT, further washed and signal was developed by Clarity Max Western ECL Substrate (BioRad #1705062) in ChemiDoc (BioRad). Details of Antibodies are as follows: ATP7B (1:1500), α-tubulin (Affinity Biosciences#AF7010, 1:20000), LAMP1 (DSHB, 1:400), LAMP2 (1:400), Rab7 (1:500), Anti-rabbit HRP (CST#7074, 1:6000), Anti-mouse HRP (CST#7076, 1:6000).

Sample preparation for ICP-OES

At 70% confluency, HepG2 cells, seeded on 60mm dishes, were treated with respective treatment conditions. After that, cells were quickly washed with 1X DPBS (Gibco #14200075) for 10 times and then were scrapped using cell scrapper. Cells were collected by centrifuging at 2000 rpm for 5 min. The cell pellete was dissolved in 100µl of 1X DPBS. After counting, 2.5 million cells were dissolved into 100 µl of ICP-OES grade 65% HNO_3 and was kept at 95ºC for overnight. Next day, 5ml of deionized water was added to it and were filtered through a

0.45-micron filter. Copper calibration is done by acid digestion of copper foil (procured from Alfa Aeasar) in 10 mL suprapure HNO_3 for 1 h. (MWD conditions: Power=400 W; Temperature=100^0C; Hold time= 1 h). From the obtained solution, different solutions of varying copper strengths (50, 75, 100, 250, 500, 1000, 5000, 10000 ppb) were prepared and were used for calibration. Copper concentration was determined using a Thermo Scientific Inductively coupled plasma optical emission spectroscopy (ICP-OES) iCAP 6500.

Cellular fractionation using sucrose gradient

For cellular fractionation, the protocol were modified from Carosi et al (Carosi et al., 2019). Cells were seeded in 100mm dishes. At 70% confluency, cells were washed in 1X DPBS and scrapped in 250µL of homogenization buffer (250 mM sucrose, 1 mM EDTA, 1X protease inhibitor cocktail, 1 mM PMSF) and lysed by pussing through 22-guage needle for 100 times. After that cells were centrifuged at 1000g for 10min at 4°C. The lysate was collected and adjusted to 1ml of 25% sucrose and 1mM EDTA solution. In a decending order of concentration the following gradient of sucrose solutions were loaded: 2.5ml of 45% sucrose solution followed by, 5.3ml of 35% and 4.2ml of 25% sucrose solution in a. 1ml of cell lysate was added at top and it was centrifuged at 1,00,000g for 2 hrs at 4°C. 1ml of fractions were collected and immunoblotting was done accordingly. Details for antibodies are as follows: ATP7B (1:1500), LAMP2 (1:400), GGA2 (BD Transduction Laboratory#612612, 1:2000), Anti-rabbit HRP (1:6000), Anti-mouse HRP (1:6000).

Time-lapse fluorescence microscopy

HepG2 cells were seeded on confocal dishes (SPL) and were co-transfected using jetPRIME (Polyplus) transfecting regent as per the manufacturer's protocol. For marking acidic compartment, cells were incubated with 0.5 mg/ml lysine-fixable dextran–Alexa Fluor 647 (Thermo #D22914) for 4 hrs followed by chasing in conjugate-free medium for 20 hrs as previously described (Bright et al., 1997). Cells were kept in imaging media during imaging. Images were acquired using Leica SP8 confocal platform using oil immersion 63X objective (NA 1.4) and deconvoluted using Leica Lightning software. Maximum Intensity Projection (MIP) was made in LAS-X software provided by Leica and videos were processed using Cyberlink Powerdirector.

Proximity ligation assay

HepG2 cell, seeded on glass coverslips, was fixed with 4% PFA after respective treatments and permeabilized with 0.1% saponin. After that, the proximity ligation assay was performed following the manufacturer's protocol (Duolink™ PLA Technology, Sigma). Cells was mounted in SIGMA Fluoroshield™ with DAPI mountant. (Sigma#F6057). Images was acquired with Leica SP8 confocal platform using oil immersion 63X objective (NA

1.4) and deconvoluted using Leica Lightning software. Details for antibodies are as follows: LAMP2 (1:100), GCC2 (1:200), ATP7B (1:200), Vps35 (SCBT#sc-374372, 1:75).

Flow cytometry Assay

At 70% confluency, HepG2 cells, seeded on 12 well plates were treated with respective treatments. After treatment, cells were washed in 1X DPBS. Lysosome was stained with 100 nM LysoTracker red DND 99 (Thermo #L7528) and cells were incubated for 30 min. LysoTracker was a kind gift from Dr. Satyam Sen Gupta (IISER Kolkata). Cells were washed with 1X DPBS and kept in 50 µL Trypsin for 10 min. After that, cells were suspended in 350 µL of FACS buffer (1XDPBS, 2% FBS, 25mM HEPES, 2mM EDTA) and was analysed by flow cytometry BD LSRFortessa (BD Biosciences). 10,000 cells were analysed for each condition. FCS Express software (version7.14.0020) was used for data analysis. Mean intensity value were used for quantification.

Image analysis and statistics

Images were analyzed in batches using ImageJ (Schneider et al., 2012), image analysis software. For colocalization study, Colocalization_Finder plugin was used. ROIs were drawn manually on best z-stack for each cell. Mender's colocalization coefficient (MCC) (MANDERS et al., 1993) and Pearson correlation coefficient(PCC) (Manders et al.; Pearson and Henrici, 1896) were used for quantifying colocalization. Merged image of LAMP2 channel and TGN46 channel was obtained in greyscale which was used to obtain the total lysosomal ATP7B. For statistical analysis and plotting, ggplot2 (Wickham, 2009, 2) and ggpubr (ggpubr package | R Documentation) package was used in R v-4.2.1 (Team, 2015). Non-parametric tests for unpaired datasets (Mann-Whitney U test) were performed for all the samples. ImagJ macro codes for image analysis are available at https://github.com/saps018/tgn-lcs

Acknowledgments

This work is supported by DBT-Wellcome Trust India Alliance Fellowship (IA/I/16/1/502369), and Core Research Grant (CRG/2021/002150) from SERB, Department of Science and Technology (DST), Government of India, and IISER-K intramural funding to AG. SM is supported by a pre-doctoral fellowship from Council of Scientific and Industrial Research (CSIR), India. The Pre-doctoral fellowship for Ruturaj is supported by Intramural Institute funding (IISER-K). We thank Amit Tuli (IMTECH, Chandigarh), Enrique Rodriguez-Boulan, Ryan Schreiner (Weill Cornell Medical College) and Carolyn Machamer (Johns Hopkins University) for sharing reagents with us.

Author contributions: AG and SM designed the experiments and wrote the manuscript. SM, Ruturaj and SD did the experiments and analysed the data. SM wrote the codes and analyzed the data. Ruturaj helped with time-lapse imaging. TG conducted the Flow cytometry experiments and analyzed the data. All authors reviewed the results and approved the final version of the manuscript.

The authors declare no competing financial interests.

538 Allison, R., J.R. Edgar, G. Pearson, T. Rizo, T. Newton, S. Günther, F. Berner, J. Hague, J.W. Connell, J. Winkler, J.
539 Lippincott-Schwartz, C. Beetz, B. Winner, and E. Reid. 2017. Defects in ER–endosome contacts impact lysosome
540 function in hereditary spastic paraplegia. *Journal of Cell Biology*. 216:1337–1355. doi:10.1083/jcb.201609033.

541 Balamurugan, K., and W. Schaffner. 2006. Copper homeostasis in eukaryotes: Teetering on a tightrope. *Biochimica et*
542 *Biophysica Acta (BBA) - Molecular Cell Research*. 1763:737–746. doi:10.1016/j.bbamcr.2006.05.001.

543 Ballabio, A., and J.S. Bonifacino. 2020. Lysosomes as dynamic regulators of cell and organismal homeostasis. *Nat Rev Mol*
544 *Cell Biol*. 21:101–118. doi:10.1038/s41580-019-0185-4.

545 Barnes, N., M.Y. Bartee, L. Braiterman, A. Gupta, V. Ustiyan, V. Zuzel, J.H. Kaplan, A.L. Hubbard, and S. Lutsenko. 2009.
546 CELL-SPECIFIC TRAFFICKING SUGGESTS A NEW ROLE FOR RENAL ATP7B IN THE INTRACELLULAR COPPER
547 STORAGE. *Traffic*. 10:767–779. doi:10.1111/j.1600-0854.2009.00901.x.

548 Barry, A.N., A. Otoikhian, S. Bhatt, U. Shinde, R. Tsivkovskii, N.J. Blackburn, and S. Lutsenko. 2011. The Lumenal Loop
549 Met672–Pro707 of Copper-transporting ATPase ATP7A Binds Metals and Facilitates Copper Release from the
550 Intramembrane Sites. *Journal of Biological Chemistry*. 286:26585–26594. doi:10.1074/jbc.M111.229039.

551 Betz, C., and M.N. Hall. 2013. Where is mTOR and what is it doing there? *Journal of Cell Biology*. 203:563–574.
552 doi:10.1083/jcb.201306041.

553 Braiterman, L.T., A. Gupta, R. Chaerkady, R.N. Cole, and A.L. Hubbard. 2015. Communication between the N and C
554 Termini Is Required for Copper-stimulated Ser/Thr Phosphorylation of Cu(I)-ATPase (ATP7B). *Journal of*
555 *Biological Chemistry*. 290:8803–8819. doi:10.1074/jbc.M114.627414.

556 Braiterman, L.T., A. Murthy, S. Jayakanthan, L. Nyasae, E. Tzeng, G. Gromadzka, T.B. Woolf, S. Lutsenko, and A.L.
557 Hubbard. 2014. Distinct phenotype of a Wilson disease mutation reveals a novel trafficking determinant in the
558 copper transporter ATP7B. *Proc. Natl. Acad. Sci. U.S.A.* 111. doi:10.1073/pnas.1314161111.

559 Bright, N.A., B.J. Reaves, B.M. Mullock, and J.P. Luzio. 1997. Dense core lysosomes can fuse with late endosomes and are
560 re-formed from the resultant hybrid organelles. *Journal of Cell Science*. 110:2027–2040.
561 doi:10.1242/jcs.110.17.2027.

562 Bull, P.C., G.R. Thomas, J.M. Rommens, J.R. Forbes, and D.W. Cox. 1993. The Wilson disease gene is a putative copper
563 transporting P–type ATPase similar to the Menkes gene. *Nat Genet*. 5:327–337. doi:10.1038/ng1293-327.

564 Carosi, J., K. Hattersly, Y. Cui, Z. Yang, R. Teasdale, and T. Sargeant. 2019. Subcellular Fractionation of Hela Cells for
565 Lysosome Enrichment Using a Continuous Percoll-density Gradient. *Bio-Protocol*. 9:1–9.
566 doi:10.21769/bioprotoc.3362.

567 Cater, M.A., S. La Fontaine, K. Shield, Y. Deal, and J.F.B. Mercer. 2006. ATP7B Mediates Vesicular Sequestration of
568 Copper: Insight Into Biliary Copper Excretion. *Gastroenterology*. 130:493–506. doi:10.1053/j.gastro.2005.10.054.

569 Char, R., and P. Pierre. 2020. The RUFYs, a Family of Effector Proteins Involved in Intracellular Trafficking and
570 Cytoskeleton Dynamics. *Front. Cell Dev. Biol.* 8:779. doi:10.3389/fcell.2020.00779.

571 Chu, B.-B., Y.-C. Liao, W. Qi, C. Xie, X. Du, J. Wang, H. Yang, H.-H. Miao, B.-L. Li, and B.-L. Song. 2015. Cholesterol
572 Transport through Lysosome-Peroxisome Membrane Contacts. *Cell*. 161:291–306.
573 doi:10.1016/j.cell.2015.02.019.

574 Cisneros, J., T.B. Belton, G.C. Shum, C.G. Molakal, and Y.C. Wong. 2022. Mitochondria-lysosome contact site dynamics
575 and misregulation in neurodegenerative diseases. *Trends in Neurosciences*. 45:312–322.
576 doi:10.1016/j.tins.2022.01.005.

577 Das, S., S. Maji, R. Raj, I. Bhattacharya, T. Saha, N. Naskar, and A. Gupta. 2020. Retromer retrieves the Wilson Disease
578 protein ATP7B from endolysosomes in a copper-dependent mode. *Journal of Cell Science*. jcs.246819.
579 doi:10.1242/jcs.246819.

580 Das, S., A. Mohammed, T. Mandal, S. Maji, J. Verma, Ruturaj, and A. Gupta. 2022. Polarized trafficking and copper
581 transport activity of ATP7B: A mutational approach to establish genotype–phenotype correlation in Wilson
582 disease. *Human Mutation*. humu.24428. doi:10.1002/humu.24428.

583 Eden, E.R. 2016. The formation and function of ER-endosome membrane contact sites. *Biochimica et Biophysica Acta*
584 *(BBA) - Molecular and Cell Biology of Lipids*. 1861:874–879. doi:10.1016/j.bbalip.2016.01.020.

585 Fanni, D., L. Pilloni, S. Orrù, P. Coni, C. Liguori, S. Serra, M.L. Lai, A. Uccheddu, L. Contu, P. Van Eyken, and G. Faa. 2005.
586 Expression of ATP7B in normal human liver. *Eur J Histochem*. 49:371–378. doi:10.4081/965.

587 ggpubr package | R Documentation.

588 Gupta, A., S. Das, and K. Ray. 2018. A glimpse into the regulation of the Wilson disease protein, ATP7B, sheds light on the
589 complexity of mammalian apical trafficking pathways. *Metallomics*. 10:378–387. doi:10.1039/C7MT00314E.

590 Gupta, A., and S. Lutsenko. 2009. Human copper transporters: mechanism, role in human diseases and therapeutic
591 potential. *Future medicinal chemistry*. 1:1125–1142. doi:10.4155/fmc.09.84.

592 Hao, F., K. Kondo, T. Itoh, S. Ikari, S. Nada, M. Okada, and T. Noda. 2017. Rheb localized on the Golgi membrane activates
593 lysosome-localized mTORC1 at the Golgi-lysosome contact site. *Journal of Cell Science*. jcs.208017.
594 doi:10.1242/jcs.208017.

595 Hasan, N.M., A. Gupta, E. Polishchuk, C.H. Yu, R. Polishchuk, O.Y. Dmitriev, and S. Lutsenko. 2012. Molecular Events
596 Initiating Exit of a Copper-transporting ATPase ATP7B from the Trans-Golgi Network. *Journal of Biological*
597 *Chemistry*. 287:36041–36050. doi:10.1074/jbc.M112.370403.

598 Hong, Z., N.M. Pedersen, L. Wang, M.L. Torgersen, H. Stenmark, and C. Raiborg. 2017. PtdIns3P controls mTORC1
599 signaling through lysosomal positioning. *Journal of Cell Biology*. 216:4217–4233. doi:10.1083/jcb.201611073.

600 Johnson, D.E., P. Ostrowski, V. Jaumouillé, and S. Grinstein. 2016. The position of lysosomes within the cell determines
601 their luminal pH. *Journal of Cell Biology*. 212:677–692. doi:10.1083/jcb.201507112.

602 Kaplan, J.H., and E.B. Maryon. 2016. How Mammalian Cells Acquire Copper: An Essential but Potentially Toxic Metal.
603 *Biophysical Journal*. 110:7–13. doi:10.1016/j.bpj.2015.11.025.

604 Kar, S., S. Sen, S. Maji, D. Saraf, Ruturaj, R. Paul, S. Dutt, B. Mondal, E. Rodriguez-Boulan, R. Schreiner, D. Sengupta, and
605 A. Gupta. 2022. Copper(II) import and reduction are dependent on His-Met clusters in the extracellular amino
606 terminus of human copper transporter-1. *Journal of Biological Chemistry*. 298:101631.
607 doi:10.1016/j.jbc.2022.101631.

608 Keren-Kaplan, T., and J.S. Bonifacino. 2021. ARL8 Relieves SKIP Autoinhibition to Enable Coupling of Lysosomes to
609 Kinesin-1. *Current Biology*. 31:540-554.e5. doi:10.1016/j.cub.2020.10.071.

610 Khatter, D., A. Sindhwani, and M. Sharma. 2015. Arf-like GTPase Arl8: Moving from the periphery to the center of
611 lysosomal biology. *Cellular Logistics*. 5:e1086501. doi:10.1080/21592799.2015.1086501.

612 Korolchuk, V.I., S. Saiki, M. Lichtenberg, F.H. Siddiqi, E.A. Roberts, S. Imarisio, L. Jahreiss, S. Sarkar, M. Futter, F.M.
613 Menzies, C.J. O'Kane, V. Deretic, and D.C. Rubinsztein. 2011. Lysosomal positioning coordinates cellular nutrient
614 responses. *Nature Cell Biology*. 13:453–462. doi:10.1038/ncb2204.

615 Kumar, G., P. Chawla, N. Dhiman, S. Chadha, S. Sharma, K. Sethi, M. Sharma, and A. Tuli. 2022. RUFY3 links Arl8b and
616 JIP4-Dynein complex to regulate lysosome size and positioning. *Nat Commun*. 13:1540. doi:10.1038/s41467-022-
617 29077-y.

618 Kuo, Y.-M., B. Zhou, D. Cosco, and J. Gitschier. 2001. The copper transporter CTR1 provides an essential function in
619 mammalian embryonic development. *Proc. Natl. Acad. Sci. U.S.A.* 98:6836–6841. doi:10.1073/pnas.111057298.

620 La Fontaine, S., and J.F.B. Mercer. 2007. Trafficking of the copper-ATPases, ATP7A and ATP7B: Role in copper
621 homeostasis. *Archives of Biochemistry and Biophysics*. 463:149–167. doi:10.1016/j.abb.2007.04.021.

622 Lim, C.-Y., O.B. Davis, H.R. Shin, J. Zhang, C.A. Berdan, X. Jiang, J.L. Counihan, D.S. Ory, D.K. Nomura, and R. Zoncu. 2019.
623 ER–lysosome contacts enable cholesterol sensing by mTORC1 and drive aberrant growth signalling in Niemann–
624 Pick type C. *Nat Cell Biol*. 21:1206–1218. doi:10.1038/s41556-019-0391-5.

625 Lim, C.-Y., and R. Zoncu. 2016. The lysosome as a command-and-control center for cellular metabolism. *Journal of Cell*
626 *Biology*. 214:653–664. doi:10.1083/jcb.201607005.

627 Lutsenko, S. 2016. Copper trafficking to the secretory pathway. *Metallomics*. 8:840–852. doi:10.1039/c6mt00176a.

628 Lutsenko, S., N.L. Barnes, M.Y. Bartee, and O.Y. Dmitriev. 2007. Function and Regulation of Human Copper-Transporting
629 ATPases. *Physiological Reviews*. 87:1011–1046. doi:10.1152/physrev.00004.2006.

630 Lutsenko, S., A. Gupta, J.L. Burkhead, and V. Zuzel. 2008. Cellular multitasking: The dual role of human Cu-ATPases in
631 cofactor delivery and intracellular copper balance. *Archives of Biochemistry and Biophysics*. 476:22–32.
632 doi:10.1016/j.abb.2008.05.005.

633 Manders, E.M.M., J. Stap, G.J. Brakenhoff, R.V. Driel, and J.A. Aten. Dynamics of three-dimensional replication patterns
634 during the S-phase, analysed by double labelling of DNA and confocal microscopy. 7.

635 MANDERS, E.M.M., F.J. VERBEEK, and J.A. ATEN. 1993. Measurement of co-localization of objects in dual-colour confocal
636 images. *Journal of Microscopy*. 169:375–382. doi:10.1111/j.1365-2818.1993.tb03313.x.

637 de Martín Garrido, N., and C.H.S. Aylett. 2020. Nutrient Signaling and Lysosome Positioning Crosstalk Through a
638 Multifunctional Protein, Folliculin. *Front. Cell Dev. Biol.* 8:108. doi:10.3389/fcell.2020.00108.

639 Marwaha, R., S.B. Arya, D. Jagga, H. Kaur, A. Tuli, and M. Sharma. 2017. The Rab7 effector PLEKHM1 binds Arl8b to
640 promote cargo traffic to lysosomes. *Journal of Cell Biology*. 216:1051–1070. doi:10.1083/jcb.201607085.

641 Michalczyk, A., E. Bastow, M. Greenough, J. Camakaris, D. Freestone, P. Taylor, M. Linder, J. Mercer, and M.L. Ackland.
642 2008. ATP7B Expression in Human Breast Epithelial Cells Is Mediated by Lactational Hormones. *J Histochem*
643 *Cytochem*. 56:389–399. doi:10.1369/jhc.7A7300.2008.

644 Miesenböck, G., D.A. De Angelis, and J.E. Rothman. 1998. Visualizing secretion and synaptic transmission with pH-
645 sensitive green fluorescent proteins. *Nature*. 394:192–195. doi:10.1038/28190.

646 Mony, V.K., S. Benjamin, and E.J. O'Rourke. 2016. A lysosome-centered view of nutrient homeostasis. *Autophagy*.
647 12:619–631. doi:10.1080/15548627.2016.1147671.

648 Oyarzún, J.E., J. Lagos, M.C. Vázquez, C. Valls, C. De la Fuente, M.I. Yuseff, A.R. Alvarez, and S. Zanlungo. 2019. Lysosome
649 motility and distribution: Relevance in health and disease. *Biochimica et Biophysica Acta (BBA) - Molecular Basis*
650 *of Disease*. 1865:1076–1087. doi:10.1016/j.bbadis.2019.03.009.

651 Payne, A.S., E.J. Kelly, and J.D. Gitlin. 1998. Functional expression of the Wilson disease protein reveals mislocalization
652 and impaired copper-dependent trafficking of the common H1069Q mutation. *Proc. Natl. Acad. Sci. U.S.A.*
653 95:10854–10859. doi:10.1073/pnas.95.18.10854.

654 Pearson, K., and O.M.F.E. Henrici. 1896. VII. Mathematical contributions to the theory of evolution.—III. Regression,
655 heredity, and panmixia. *Philosophical Transactions of the Royal Society of London. Series A, Containing Papers of*
656 *a Mathematical or Physical Character*. 187:253–318. doi:10.1098/rsta.1896.0007.

657 Peña, K., J. Coblenz, and K. Kiselyov. 2015. Brief exposure to copper activates lysosomal exocytosis. *Cell Calcium*. 57:257–
658 262. doi:10.1016/j.ceca.2015.01.005.

659 Peña, K.A., and K. Kiselyov. 2015. Transition metals activate TFEB in overexpressing cells. *Biochemical Journal*. 470:65–
660 76. doi:10.1042/BJ20140645.

661 Petrukhin, K., S. Lutsenko, I. Chernov, B.M. Ross, J.H. Kaplan, and T.C. Gilliam. 1994. Characterization of the Wilson
662 disease gene encoding a P-type copper transporting ATPase: genomic organization, alternative splicing, and
663 structure/function predictions. *Hum Mol Genet*. 3:1647–1656. doi:10.1093/hmg/3.9.1647.

664 Polishchuk, E.V., M. Concilli, S. Iacobacci, G. Chesi, N. Pastore, P. Piccolo, S. Paladino, D. Baldantoni, S.C.D. van
665 IJzendoorn, J. Chan, C.J. Chang, A. Amoresano, F. Pane, P. Pucci, A. Tarallo, G. Parenti, N. Brunetti-Pierri, C.
666 Settembre, A. Ballabio, and R.S. Polishchuk. 2014. Wilson disease protein ATP7B utilizes lysosomal exocytosis to
667 maintain copper homeostasis. *Dev Cell*. 29:686–700. doi:10.1016/j.devcel.2014.04.033.

668 Polishchuk, E.V., A. Merolla, J. Lichtmannegger, A. Romano, A. Indrieri, E.Y. Ilyechova, M. Concilli, R. De Cegli, R. Crispino,
669 M. Mariniello, R. Petruzzelli, G. Ranucci, R. Iorio, F. Pietrocola, C. Einer, S. Borchard, A. Zibert, H.H. Schmidt, E. Di
670 Schiavi, L.V. Puchkova, B. Franco, G. Kroemer, H. Zischka, and R.S. Polishchuk. 2019. Activation of Autophagy,
671 Observed in Liver Tissues From Patients With Wilson Disease and From ATP7B-Deficient Animals, Protects
672 Hepatocytes From Copper-Induced Apoptosis. *Gastroenterology*. 156:1173-1189.e5.
673 doi:10.1053/j.gastro.2018.11.032.

674 Polishchuk, E.V., and R.S. Polishchuk. 2016. The emerging role of lysosomes in copper homeostasis. *Metallomics*. 8:853–
675 862. doi:10.1039/C6MT00058D.

676 Polishchuk, R., and S. Lutsenko. 2013. Golgi in copper homeostasis: a view from the membrane trafficking field.
677 *Histochemistry and Cell Biology*. 140:285–295. doi:10.1007/s00418-013-1123-8.

678 Polishchuk, R.S., and E.V. Polishchuk. 2019. From and to the Golgi – defining the Wilson disease protein road map. *FEBS*
679 *Lett*. 593:2341–2350. doi:10.1002/1873-3468.13575.

680 Pols, M.S., E. van Meel, V. Oorschot, C. ten Brink, M. Fukuda, M.G. Swetha, S. Mayor, and J. Klumperman. 2013. hVps41
681 and VAMP7 function in direct TGN to late endosome transport of lysosomal membrane proteins. *Nat Commun*.
682 4:1361. doi:10.1038/ncomms2360.

683 Pu, J., C.M. Guardia, T. Keren-Kaplan, and J.S. Bonifacino. 2016. Mechanisms and functions of lysosome positioning.
684 *Journal of Cell Science*. jcs.196287. doi:10.1242/jcs.196287.

685 Puertollano, R. 2014. mTOR and lysosome regulation. *F1000Prime Rep*. 6. doi:10.12703/P6-52.

686 Purkait, K., Ruturaj, A. Mukherjee, and A. Gupta. 2019. ATP7B Binds Ruthenium(II) *p* -Cymene Half-Sandwich Complexes:
687 Role of Steric Hindrance and Ru–I Coordination in Rescuing the Sequestration. *Inorg. Chem.* 58:15659–15670.
688 doi:10.1021/acs.inorgchem.9b02780.

689 Raiborg, C., E.M. Wenzel, and H. Stenmark. 2015. ER –endosome contact sites: molecular compositions and functions.
690 *EMBO J*. 34:1848–1858. doi:10.15252/embj.201591481.

691 Rowland, A.A., P.J. Chitwood, M.J. Phillips, and G.K. Voeltz. 2014. ER Contact Sites Define the Position and Timing of
692 Endosome Fission. *Cell*. 159:1027–1041. doi:10.1016/j.cell.2014.10.023.

693 Sancak, Y., L. Bar-Peled, R. Zoncu, A.L. Markhard, S. Nada, and D.M. Sabatini. 2010. Ragulator-Rag Complex Targets
694 mTORC1 to the Lysosomal Surface and Is Necessary for Its Activation by Amino Acids. *Cell*. 141:290–303.
695 doi:10.1016/j.cell.2010.02.024.

696 Schneider, C.A., W.S. Rasband, and K.W. Eliceiri. 2012. NIH Image to ImageJ: 25 years of image analysis. *Nature methods*.
697 9:671–5. doi:10.1038/NMETH.2089.

698 Settembre, C., A. Fraldi, D.L. Medina, and A. Ballabio. 2013. Signals from the lysosome: a control centre for cellular
699 clearance and energy metabolism. *Nat Rev Mol Cell Biol*. 14:283–296. doi:10.1038/nrm3565.

700 Söderberg, O., M. Gullberg, M. Jarvius, K. Ridderstråle, K.-J. Leuchowius, J. Jarvius, K. Wester, P. Hydbring, F. Bahram, L.-
701 G. Larsson, and U. Landegren. 2006. Direct observation of individual endogenous protein complexes in situ by
702 proximity ligation. *Nat Methods*. 3:995–1000. doi:10.1038/nmeth947.

703 Stewart, D.J., K.K. Short, B.N. Maniaci, and J.L. Burkhead. 2019. COMMD1 and PtdIns(4,5)P2 interaction maintain ATP7B
704 copper transporter trafficking fidelity in HepG2 cells. *Journal of Cell Science*. jcs.231753. doi:10.1242/jcs.231753.

705 Team, R.D.C. 2015. R: A language and environment for statistical computing. R Foundation for Statistical Computing,
706 Vienna, Austria. URL http://www.R-project.org/. *R Foundation for Statistical Computing, Vienna, Austria.*
707 doi:10.1007/978-3-540-74686-7.

708 Wickham, H. 2009. Ggplot2 : elegant graphics for data analysis. Springer. 212 pp.

709 Zhou, D., S. Jia, L. Yi, Z. Wu, Y. Song, B. Zhang, Y. Li, X. Yang, A. Xu, X. Li, W. Zhang, W. Duan, Z. Li, S. Qi, Z. Chen, Q.
710 Ouyang, J. Jia, J. Huang, X. Ou, and H. You. 2022. Identification of potential modifier genes in Chinese patients
711 with Wilson disease. *Metallomics*. 14:mfac024. doi:10.1093/mtomcs/mfac024.

712 Zhou, L., X. Xue, K. Yang, Z. Feng, M. Liu, and J.C. Pastor-Pareja. 2023. Convergence of secretory, endosomal, and
713 autophagic routes in trans-Golgi–associated lysosomes. *Journal of Cell Biology*. 222:e202203045.
714 doi:10.1083/jcb.202203045.

715

716

Legends to Figures:

Figure 1: ATP7B distribution at the TGN and endolysosomes in different copper treatments. (A) Immunofluorescence image of ATP7B (green) in HepG2 cell line co-stained with endolysosomal marker LAMP2 (red) and TGN marker TGN46 (blue) shows presence of ATP7B on both the compartments, irrespective of cellular copper condition i.e., basal, high copper (100µM Cu) as well as copper chelated conditions (25µM TTM, 100µM BCS). The marked area on 'merge' panel is enlarged in 'inset'. The arrowhead shows colocalisation between ATP7B-LAMP2, the asterisk shows colocalisation between ATP7B-TGN46. The scale bar: 5µm. **(B)** The Pearson's Colocalisation Coefficient (PCC) between ATP7B-TGN46 and ATP7B-LAMP2 in different copper condition are demonstrated by box plot with jitter points. The box represents the 25th to 75th percentiles, and the median in the middle. The whiskers show the data points within the range of 1.5 × interquartile range (IQR) from the first and third quartile. $*p < 0.05$, $**p < 0.01$, $****p < 0.0001$; ns, not significant (nonparametric Mann–Whitney U test/Wilcoxon rank-sum test). The black * shows the comparison of colocalisation between ATP7B-TGN46 and ATP7B-LAMP2. The green * shows the comparison of ATP7B-TGN46 colocalisation under different condition with the basal. The orange * shows the comparison of ATP7B-LAMP2 colocalisation under different condition with the basal. **(C)** Total fraction of ATP7B present in TGN46 and LAMP2 positive compartment are demonstrated by box plot with jitter points. The box represents the 25th to 75th percentiles, and the median in the middle. The whiskers show the data points within the range of 1.5 × interquartile range (IQR) from the first and third quartile. ns, not significant (nonparametric Mann–Whitney U test/Wilcoxon rank-sum test) with respect to Basal. Sample size (N) for (B) and (C) are TTM: 42, BCS: 57, Basal: 24, Cu20: 44, Cu100: 49, Cu250: 50. **(D)** comparison of copper accumulation in HepG2 cells (n = 9) under different treatment conditions shows elevated copper accumulation in case of increased copper treatment, copper concentrations were measured in parts per billion (ppb, mean ± SD) $**p < 0.01$; $***p < 0.001$; ns, not significant (nonparametric Mann–Whitney U test/Wilcoxon rank-sum test). **(E)** Immunoblot of ATP7B after different copper treatment. α-tubulin has been used as a housekeeping control. The fold changes of ATP7B abundance normalized against α-tubulin has been mentions **(F)** Sucrose gradient fractions (1-4) show that presence of ATP7B in both the Golgi fraction (GGA2) and endolysosomal fraction (LAMP2) at basal condition.

Figure 2: Distribution of ATP7B and ATP7A in hepatic and non-hepatic cell lines. (A) Immunofluorescence image of ATP7B (green) in Huh7 cell line co-stained with LAMP2 (red) and TGN46 (blue) shows presence of ATP7B on both the compartments, irrespective of cellular copper conditions. The marked area on 'merge' panel is enlarged in 'inset'. The arrowhead shows colocalisation between ATP7B-LAMP2. **(B)** The PCC between ATP7B-TGN46 and ATP7B-LAMP2 in different copper condition are demonstrated by box plot with jitter points. The box represents the 25th to 75th percentiles, and the median in the middle. The whiskers show the data points

within the range of 1.5 × interquartile range (IQR) from the first and third quartile. The comparison of colocalisation between ATP7B-TGN46 and ATP7B-LAMP2 is shown as $***p < 0.001$, $****p < 0.0001$; ns, not significant (nonparametric Mann–Whitney U test/Wilcoxon rank-sum test). **(C)** Total fraction of ATP7B present in TGN46 and LAMP2 compartment are demonstrated by box plot with jitter points. The box represents the 25th to 75th percentiles, and the median in the middle. The whiskers show the data points within the range of 1.5 × interquartile range (IQR) from the first and third quartile. $*p < 0.05$, $****p < 0.0001$; ns, not significant (nonparametric Mann–Whitney U test/Wilcoxon rank-sum test) with respect to Basal. Sample size (N) for (B) and (C) are BCS: 45, Basal: 42, Cu100: 25. **(D)** Immunoblot of cell lysates shoes presence of endogenous ATP7B in different cell lines. α-tubulin has been used as housekeeping protein. **(E)** Immunofluorescence image of ATP7B (green) in HeLa cell line co-stained with LAMP2 (red) and TGN46 (blue) shows different localization pattern of ATP7B that hepatocytes. The marked area on 'merge' panel is enlarged in 'inset'. The arrowhead shows colocalisation between ATP7B-LAMP2, the asterisk shows colocalisation between ATP7B and TGN46. **(F)** The PCC between ATP7B-TGN46 and ATP7B-LAMP2 in different copper condition are demonstrated by box plot with jitter points. The box represents the 25th to 75th percentiles, and the median in the middle. The whiskers show the data points within the range of 1.5 × interquartile range (IQR) from the first and third quartile. $****p < 0.0001$; (nonparametric Mann–Whitney U test/Wilcoxon rank-sum test). Sample size (N) for (E) are Basal: 36 Cu: 36. (G) Ectopically expressed mKO-ATP7A (red) in HepG2 co-stained with ATP7B (green) and TGN46 (blue) (*top panel*) and LAMP2 (green) and TGN46 (blue) (*bottom panel*) shows different localization pattern of ATP7A than ATP7B. The marked area on 'merge' panel is enlarged in 'inset'. Asterisk marks the nucleus of the cells. [Scale bar: 5µm.]

Figure 3: ATP7B localization at TGN-proximal lysosomes. (A) 3D rendered image of ATP7B (green) co-stained with LAMP2 (red) and TGN46 (blue) shows ATP7B localization in TGN46-LAMP2 proximity region in HepG2 cells. **(B)** STED image of ATP7B (green) co-stained with TGN46 (blue) and LAMP2 (red) shown presence of ATP7B in TGN46-LAMP2 colocalising region, both in basal (top) and Cu (bottom) treated conditions (marked with arrowhead). Marked area in the first panel is enlarged in the next panels. **(C)** Proximity ligation assay shows presence of ectopically expressed mEGFP-ATP7B (green) on the GCC2-LAMP2 PLA positive region (red), both in basal (left) and Cu (right) treated conditions (marked with arrowhead). For each conditions, marked regions on the left are enlarged in the next. [Scale bar: 5µm.]

Figure 4: **ATP7B localization at the TGN and lysosomes and at TGN-lysosomes hybrid compartments upon TGN disruption**. **(A)** Ectopically expressed mEGFP-ATP7B (green) is co-expressed with dsRed-GalT (red). Acidic compartments are marked with Dextran (blue). ATP7B is localized in the region where Golgi (red) and acidic compartment (blue) colocalises shows ATP7B is present on true TGN-proximal lysosome (marked with

arrowhead). **(B)** GLCS is marked with LAMP1 (green) and GM130 (red) colocalisation, (marked with asterisk). TGN-lysosome proximity region is marked with LAMP1 (green) and GM130 (red) colocalisation, (marked with arrowhead). **(C)** ATP7B (green) co-stained with LAMP1 (red) and cis-Golgi marker GM130 (blue) shows absence of ATP7B in the GLCS. **(D)** Immunofluorescence image of ATP7B (green) in HepG2 cell line (control, *top panel* or Brefeldin-A treated, *bottom panel*) co-stained with LAMP2 (red) and TGN46 (blue) shows that Brefeldin-A treatment results in formation of TGN46-LAMP2 hybrid organelle and presence of ATP7B there, marked with arrow (bottom panel). **(E)** The PCC between ATP7B-TGN46 and ATP7B-LAMP2 in basal and copper conditions in control, ct (green) and BFA (orange) treated conditions are demonstrated by box plot with jitter points. The box represents the 25th to 75th percentiles, and the median in the middle. The whiskers show the data points within the range of 1.5 × interquartile range (IQR) from the first and third quartile. $****p < 0.000$ (nonparametric Mann–Whitney U test/Wilcoxon rank-sum test). Sample size (N) are ct: 43, BFA: 63. **(F)** Subdomain of TGN based on pH is marked by ratiometric pHluorin tagged TGN38 in blue (low acidity) and green (acidic). [Scale bar: 1µm] Line image shows the relative position of all the proteins. [The scale bar for rest of the figures: 5µm.]

Figure 5: TGN-proximal lysosome plays a role in endo-lysosomal sorting of wt-ATP7B and WD causing ATP7B mutants. (A) PCC between TGN46-LAMP2 shows increased colocalisation upon copper treatment. The data is represented as box plot with jitter points. The box represents the 25th to 75th percentiles, and the median in the middle. The whiskers show the data points within the range of 1.5 × interquartile range (IQR) from the first and third quartile. $**p < 0.01$, $****p < 0.0001$ (nonparametric Mann–Whitney U test/Wilcoxon rank-sum test). Sample size (N) for Basal: 24, Cu20: 44, Cu100: 49, Cu250: 50. **(B)** Regression model shows a positive relationship between TGN46-LAMP2 and ATP7B-LAMP2 PCC values. **(C)** Time lapse imaging of ectopically expressed mEGFP-ATP7B (green) co-transfected with dsRed-GalT (red). Acidic compartments are marked with Dextran (blue). Arrowhead shows pinching off of ATP7B from Golgi to a Dextran positive vesicle. Time scales are in minutes (D) ectopically expressed mEGFP-ATP7B (wt, H1069Q, and S653Y) co-stained with LAMP2 (red) and TGN46 (blue) shows presence of Golgi exiting ATP7B in TGN46-LAMP2 colocalising region.

Figure 6: Lysosomal positioning regulates ATP7B abundance at the TGN-proximal lysosome. (A) Immunostaining of ATP7B (green) co-stained with LAMP2 (red) and TGN46 (blue) in HepG2 transfected (Tr) with GFP-Arl8b (i), and GFP-RUFY3 (iv) in un-transfected cells (UT). Boundaries of transfected cells are marked with white line. Asterisk marks the nucleus of the cells. The PCC between ATP7B-TGN46 (ii), (v); and TGN46-LAMP2 (iii), (vi) in transfected and un-transfected cells are demonstrated by box plot with jitter points. The box represents the 25th to 75th percentiles, and the median in the middle. The whiskers show the data points within the range of 1.5 × interquartile range (IQR) from the first and third quartile. $*p < 0.05$, ns: not significant

(nonparametric Mann–Whitney U test/Wilcoxon rank-sum test). Sample size (N) for GFP-Arl8b (i) are Tr: 20, UT: 38; GFP-RUFY3 (ii) are Tr: 14, UT: 42 **(B)** (i) Immunofluorescence image of ATP7B (green) in HepG2 cell line co-stained with LAMP2 (red) and TGN46 (blue) shows that Rapamycin treatment results in increased ATP7B localization in endolysosomes there, marked with arrowhead (bottom). The PCC between (ii) ATP7B-LAMP2 and (iii) TGN46-LAMP2 in basal and copper conditions in ct (green) and Rapamycin (orange) treated conditions are demonstrated by box plot with jitter points. The box represents the 25th to 75th percentiles, and the median in the middle. The whiskers show the data points within the range of 1.5 × interquartile range (IQR) from the first and third quartile. $****p < 0.000$ (nonparametric Mann–Whitney U test/Wilcoxon rank-sum test). Sample size (N) are ct: 43, Rapa: 37. [The scale bar: 5µm.] **(C), (D)** Immunoblotting and subsequent quantitation of LAMP1, LAMP2 and Rab7 in basal and copper treated condition shows lysosomal biogenesis upon 2hr copper treatment. **(E)** Flow cytometry analysis shows increase in Lysotracker intensity upon copper treatment.

Figure 7: Vesicularized ATP7B recycles back to perinuclear lysosomes and TGN-proximal lysosome upon copper chelation. (A) Time lapse imaging of ectopically expressed mKO-ATP7B (red) co-transfected with pHluorin tagged TGN38 (green). Acidic compartments are marked with Dextran (blue). Time scales are in minutes. **(B)** Immunostaining of ATP7B (green) co-stained with LAMP2 (red) and TGN46 (blue) in HepG2 in control and CHX treated conditions in different copper conditions i.e., basal, Cu250 and Cu250>BCS, 2hr. The arrowhead shows colocalisation between ATP7B-LAMP2, the asterisk shows colocalisation between ATP7B-TGN46. The PCC between ATP7B-LAMP2 **(C)** and ATP7B-TGN46 **(D)** in ct and CHX treated cells under different copper conditions are demonstrated by box plot with jitter points. The box represents the 25th to 75th percentiles, and the median in the middle. The whiskers show the data points within the range of 1.5 × interquartile range (IQR) from the first and third quartile. $***p < 0.001$, $****p < 0.0001$; ns, not significant (nonparametric Mann–Whitney U test/Wilcoxon rank-sum test). Sample size (N) for (C) and (D) in basal condition are basal: 94, Cu250: 108, Cu_BCS30m: 104, Cu_BCS2hr: 99. Sample size for CHX treated condition are basal: 57, Cu250: 84, Cu_BCS30m: 100, Cu_BCS2hr: 103. [scale bar: 5µm.]

Fig 8: Vesicularized ATP7B recycles back to peri-Golgi lysosomes and TGN-proximal lysosome upon copper depletion. (A) Model representing peri-Golgi region that harbors the peri-Golgi lysosomes **(B)** Quantitation of Localization of ATP7B in peri-Golgi region upon copper treatment and subsequent copper chelation. The box represents the 25th to 75th percentiles, and the median in the middle. The whiskers show the data points within the range of 1.5 × interquartile range (IQR) from the first and third quartile. $*p < 0.05$, $**p < 0.01$, $***p < 0.001$, $****p < 0.0001$; ns, not significant (nonparametric Mann–Whitney U test/Wilcoxon rank-sum test). Sample size (N) in basal condition are basal: 80, Cu250: 100, Cu_BCS30m: 95, Cu_BCS2hr: 86. **(C)**

Model illustrating the copper-induced trafficking of ATP7B between perinuclear and peripheral lysosomes and its localization at the TGN-proximal lysosome.

Supplementary figure legends

Figure S1: (A) Immunofluorescence image of ATP7B (green) in HepG2 cell line co-stained with endolysosomal marker LAMP2 (red) and TGN marker TGN46 (blue) in high and low copper conditions (20µM Cu, 250µM Cu). The marked area on 'merge' panel is enlarged in 'inset'. The arrowhead shows colocalisation between ATP7B-LAMP2, the asterisk shows colocalisation between ATP7B-TGN46. The scale bar: 5µm. **(B)** The fraction of ATP7B in TGN46 and LAMP2 in different copper condition are demonstrated by box plot with jitter points. The box represents the 25th to 75th percentiles, and the median in the middle. The whiskers show the data points within the range of 1.5 × interquartile range (IQR) from the first and third quartile. $*p < 0.05$, $**p < 0.01$, $****p < 0.0001$; ns, not significant (nonparametric Mann–Whitney U test/Wilcoxon rank-sum test). The black * shows the comparison of colocalisation between ATP7B-TGN46 and ATP7B-LAMP2. The green * shows the comparison of ATP7B-TGN46 colocalisation under different condition with the basal. The orange * shows the comparison of ATP7B-LAMP2 colocalisation under different condition with the basal. Sample size (N) are TTM: 42, BCS: 57, Basal: 24, Cu20: 44, Cu100: 49, Cu250: 50.

Figure S2: (A) Immunofluorescence image of ATP7B (green) in HepG2 cell line co-stained with endolysosomal marker LAMP2 (red) and TGN marker TGN46 (blue) shows presence of ATP7B on both the compartments, irrespective of cellular copper condition i.e. basal, high copper (20µM Cu, 100µM Cu and 250µM Cu) as well as copper chelated conditions (25µM TTM, 100µM BCS). The marked area on 'merge' panel is enlarged in 'inset'. The white arrow shows colocalisation between ATP7B-LAMP2, the asterisk shows colocalisation between ATP7B-TGN46. Scale bar: 5µm. **(B)** The fraction of ATP7B in TGN46 and LAMP2 in different copper condition are demonstrated by box plot with jitter points. The box represents the 25th to 75th percentiles, and the median in the middle. The whiskers show the data points within the range of 1.5 × interquartile range (IQR) from the first and third quartile. The comparison of colocalisation between ATP7B-TGN46 and ATP7B-LAMP2 are denoted as $*p < 0.05$, $***p < 0.001$, $****p < 0.0001$; ns, not significant (nonparametric Mann–Whitney U test/Wilcoxon rank-sum test). Sample size (N) for TTM: 46, BCS: 33, Basal: 36, Cu20: 23, Cu100: 33, Cu250: 67.

Fig S3: Immunofluorescence image of ectopically expressed mEGFP-ATP7B (green) in HEK293T cell line **(A)** and endogenous ATP7B (green) in HeLa cells **(B)** co-stained with LAMP2 (red) and TGN46 (blue) shows different localization pattern of ATP7B that hepatocytes. The marked area on 'merge' panel is enlarged in 'inset'. The arrowhead shows colocalisation between ATP7B-LAMP2, the asterisk shows colocalisation between ATP7B-TGN46. [Scale bar: 5µm.] **(C)** Ectopically expressed mKO-ATP7A (red) in HepG2 cell co-stained with

ATP7B (green) and TGN46 (blue) under Cu treated condition. The arrowhead marks the membrane localization of ATP7A under copper treated condition.

Fig S4: Immunofluorescence of ATP7B (green) co-stained with different TGN-endolysosome combinations i.e. **(A)** LAMP1(red)-TGN46(blue), **(B)** LAMP1(red)-Golgin97(blue), **(C)** LAMP2(red)-TGN38(blue) shows presence of ATP7B in TGN marker –endolysosome marker colocalising regions (marked with arrowhead). **(D)** Though, ATP7B was absent in Rab7(red)-TGN46(blue) colocalisation region (marked with arrow). **(E)** Presence of ATP7B in TGN-proximal lysosome in Huh7 cell is marked by co-staining ATP7B (green), LAMP2 (red) and TGN46 (blue). **(F)** Immunofluorescence image of negative (only GCC2, only LAMP2, no antibody) and positive control (ATP7B/Vps35) for PLA. [Scale bar: 5µm.]

Fig S5: (A) TGN-lysosome proximity region is shown by colocalisation of TGN46 (blue) with LAMP1 (green, colocalising region marked with asterisk) and LAMP2 (red, colocalising region marked with arrowhead). **(B)** Colocalisation between TGN46-LAMP2 shows increased colocalisation in BFA treated cells than control (ct). Data represented by box plot with jitter points. The box represents the 25th to 75th percentiles, and the median in the middle. The whiskers show the data points within the range of 1.5 × interquartile range (IQR) from the first and third quartile. $****p < 0.000$ (nonparametric Mann–Whitney U test/Wilcoxon rank-sum test). Sample size (N) are ct: 43, BFA: 63. **(C)** Cells ectopically expressing GFP-Arl8b and GFP-RUFY3 are shown in magenta. **(D)** Immunostaining of ATP7B (green) co-stained with LAMP2 (red) and TGN46 (blue) in HepG2 in control and CHX treated conditions in Cu250>BCS 30min treatment. The arrowhead shows colocalisation between ATP7B-LAMP2, the asterisk shows colocalisation between ATP7B-TGN46. **(E)** The fraction of ATP7B present in LAMP2 and TGN46 in ct and CHX treated cells under different copper conditions are demonstrated by box plot with jitter points. The box represents the 25th to 75th percentiles, and the median in the middle. The whiskers show the data points within the range of 1.5 × interquartile range (IQR) from the first and third quartile. $*p < 0.05$, $****p < 0.0001$; ns, not significant (nonparametric Mann–Whitney U test/Wilcoxon rank-sum test). **(F)** The PCC between ATP7B-LAMP2 and ATP7B-TGN46 in ct and CHX treated cells under different copper conditions are demonstrated by box plot with jitter points. The box represents the 25th to 75th percentiles, and the median in the middle. The whiskers show the data points within the range of 1.5 × interquartile range (IQR) from the first and third quartile. $*p < 0.05$, $**p < 0.01$, $***p < 0.001$, $****p < 0.0001$; ns, not significant (nonparametric Mann–Whitney U test/Wilcoxon rank-sum test). Sample size (N) for (E) and (F) in basal condition are basal: 94, Cu250: 108, Cu_BCS30m: 104, Cu_BCS2hr: 99. Sample size for CHX treated condition are basal: 57, Cu250: 84, Cu_BCS30m: 100, Cu_BCS2hr: 103. [Scale bar: 5µm.]

Fig 1

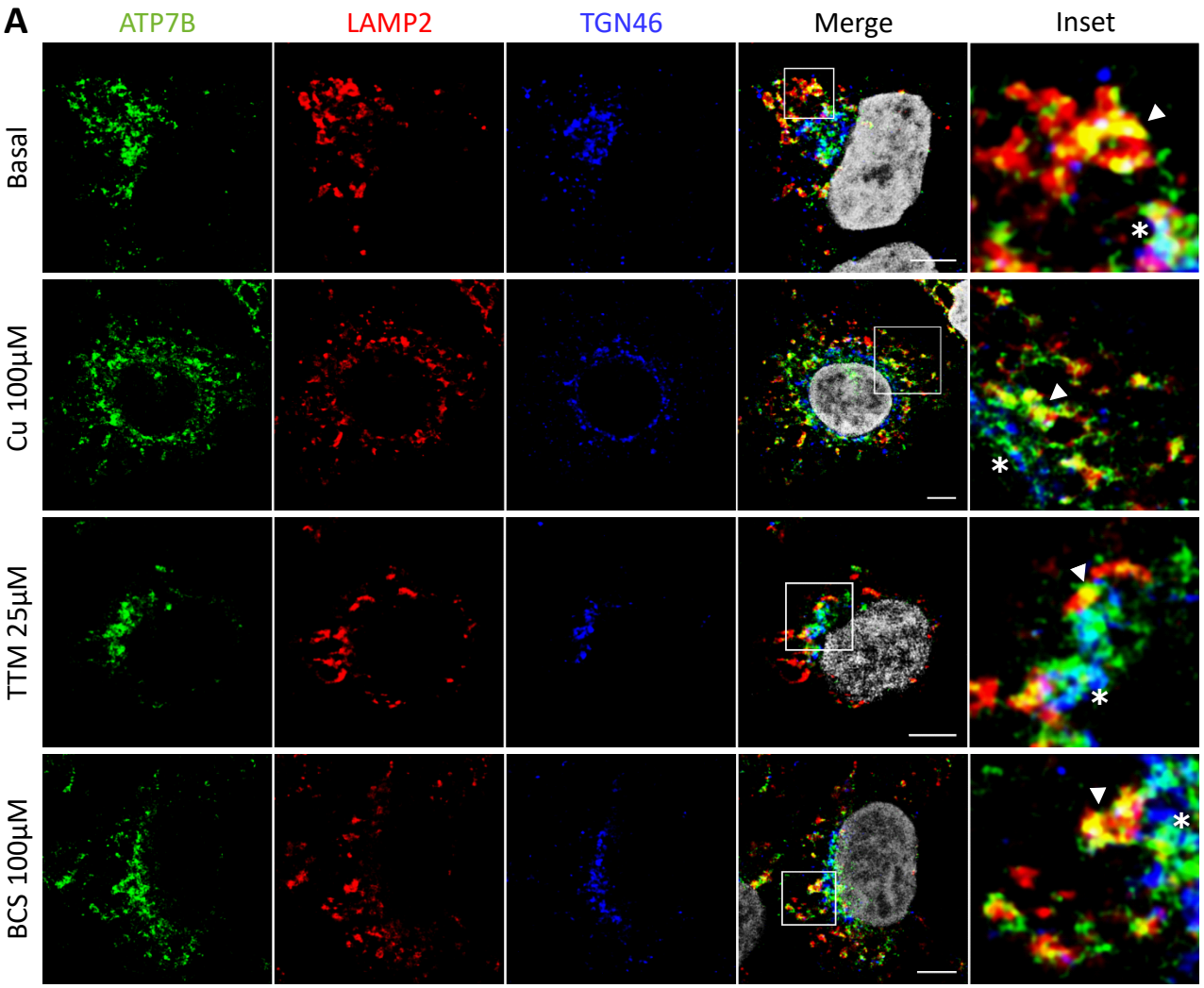
A
ATP7B
LAMP2
TGN46
Merge
Inset
Basal
Cu 100µM
TTM 25µM
BCS 100µM

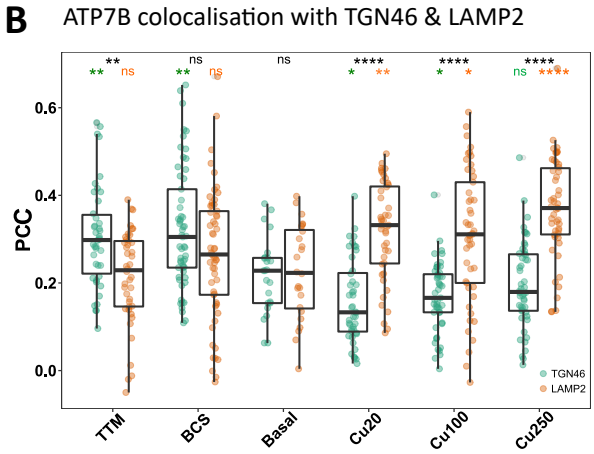
B
ATP7B colocalisation with TGN46 & LAMP2
PCC
0.0
0.2
0.4
0.6
TTM
BCS
Basal
Cu20
Cu100
Cu250
TGN46
LAMP2

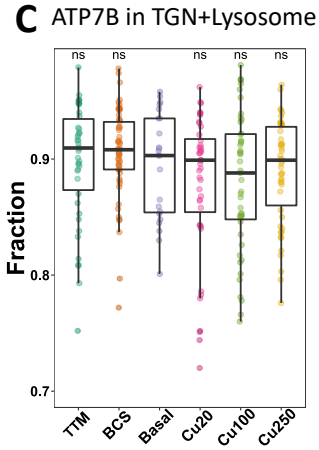
C
ATP7B in TGN+Lysosome
Fraction
0.7
0.8
0.9
TTM
BCS
Basal
Cu20
Cu100
Cu250

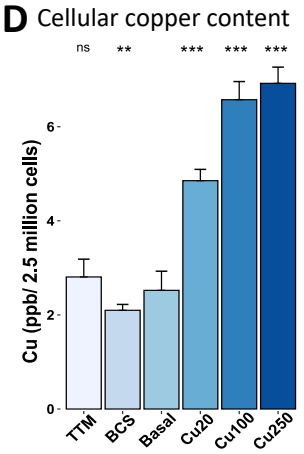
D
Cellular copper content
Cu (ppb/ 2.5 million cells)
0
2
4
6
TTM
BCS
Basal
Cu20
Cu100
Cu250

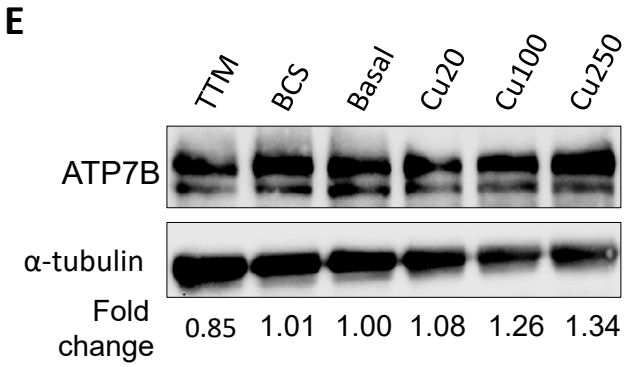
E
TTM
BCS
Basal
Cu20
Cu100
Cu250
ATP7B
α-tubulin
Fold change
0.85
1.01
1.00
1.08
1.26
1.34

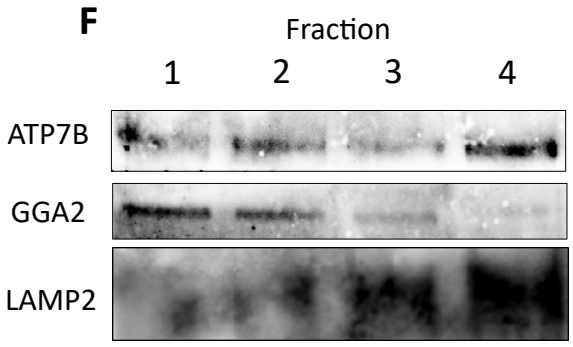
F
Fraction
1
2
3
4
ATP7B
GGA2
LAMP2

Fig 2

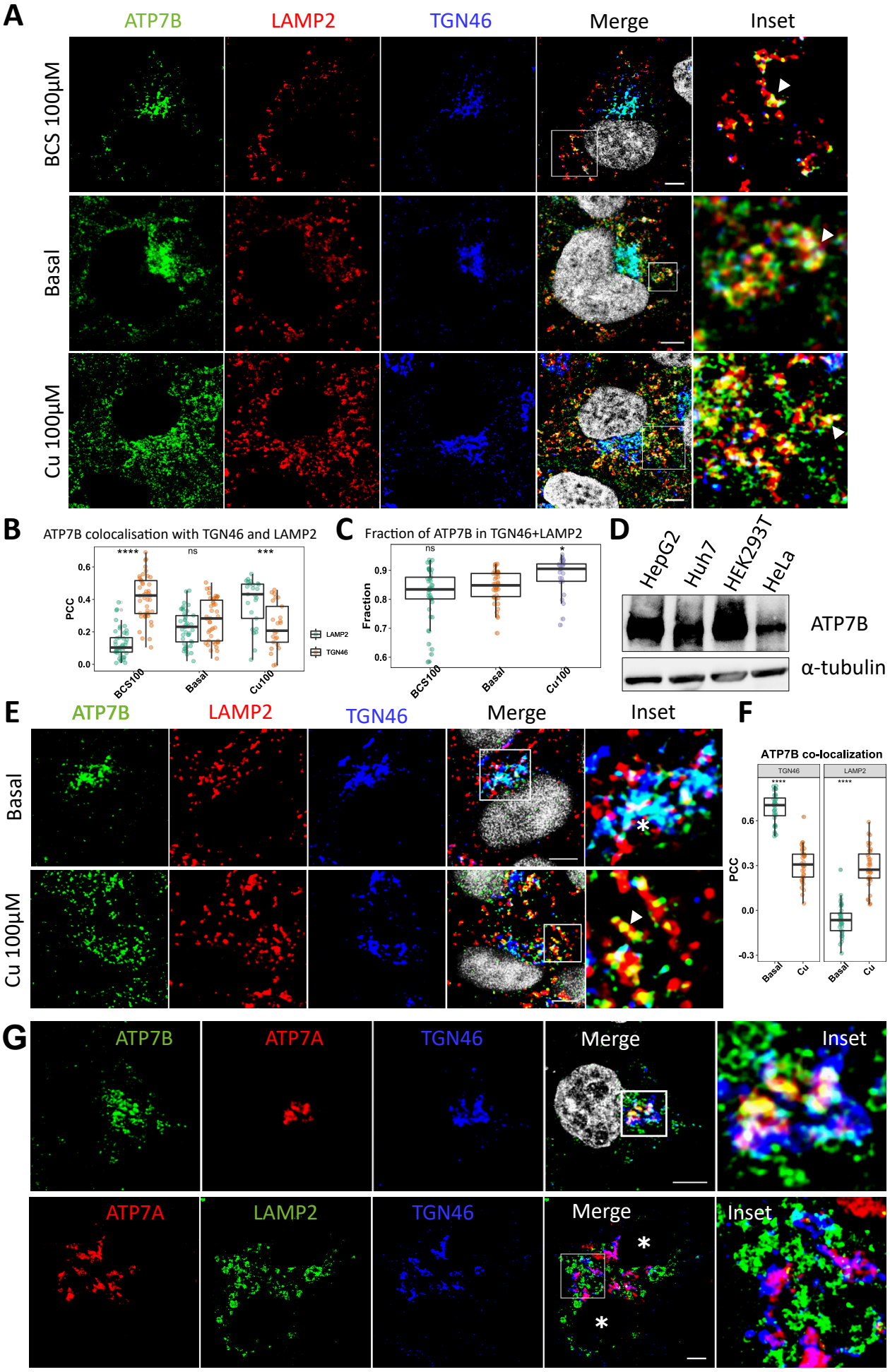
A
ATP7B
LAMP2
TGN46
Merge
Inset
BCS 100µM
Basal
Cu 100µM
B
ATP7B colocalisation with TGN46 and LAMP2
PCC
BCS100
Basal
Cu100
LAMP2
TGN46
C
Fraction of ATP7B in TGN46+LAMP2
Fraction
D
HepG2
Huh7
HEK293T
HeLa
ATP7B
α-tubulin
E
F
ATP7B co-localization
TGN46
LAMP2
G
ATP7A

Fig 3

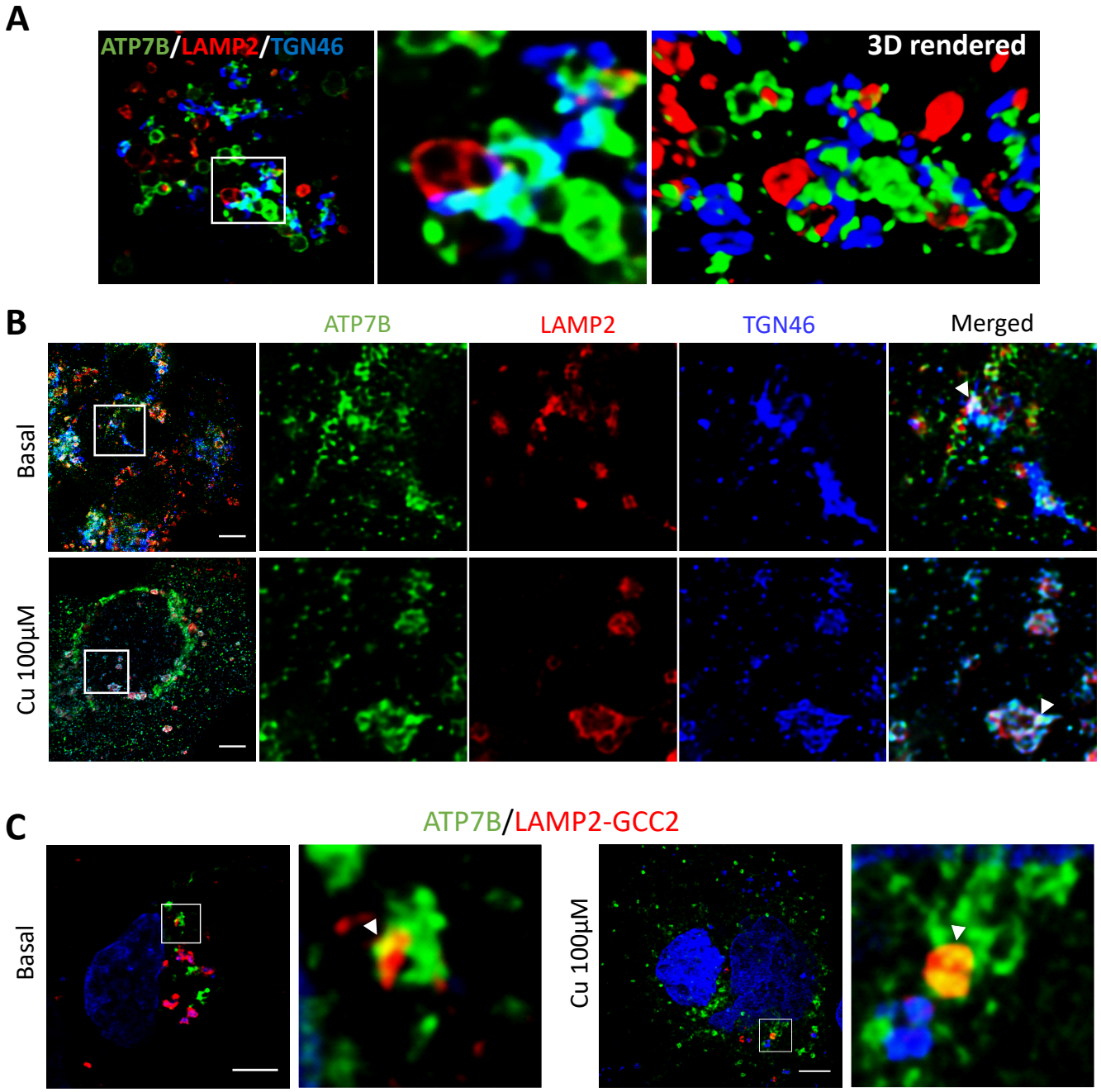
A
ATP7B/LAMP2/TGN46
3D rendered
B
ATP7B
LAMP2
TGN46
Merged
Basal
Cu 100μM
C
ATP7B/LAMP2-GCC2
Basal
Cu 100μM

Fig 4

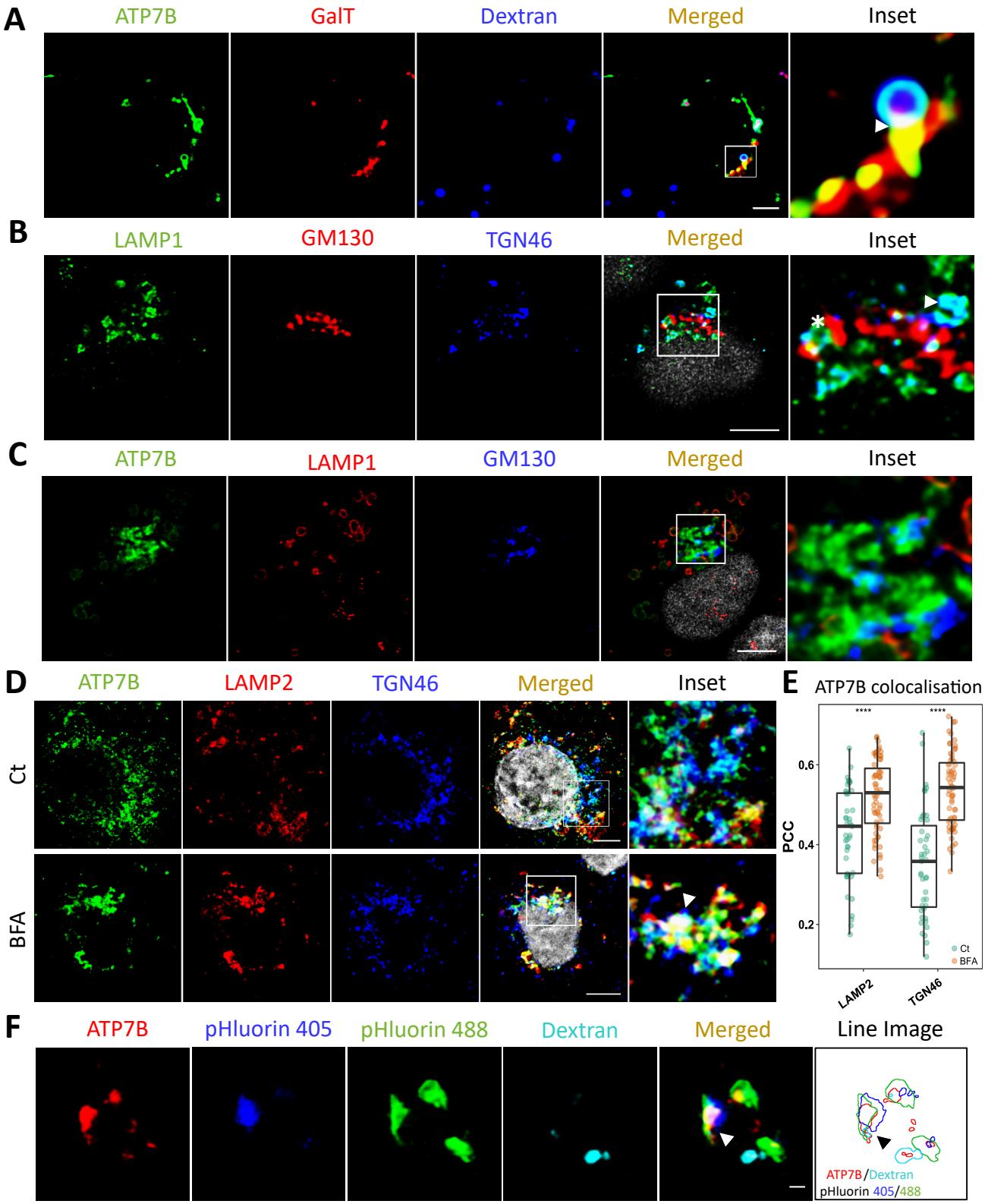
A
ATP7B
GalT
Dextran
Merged
Inset
B
LAMP1
GM130
TGN46
Merged
Inset
C
ATP7B
LAMP1
GM130
Merged
Inset
D
ATP7B
LAMP2
TGN46
Merged
Inset
Ct
BFA
E
ATP7B colocalisation
PCC
0.6
0.4
0.2
****
****
Ct
BFA
LAMP2
TGN46
F
ATP7B
pHluorin 405
pHluorin 488
Dextran
Merged
Line Image
ATP7B/Dextran
pHluorin 405/488

Fig 5

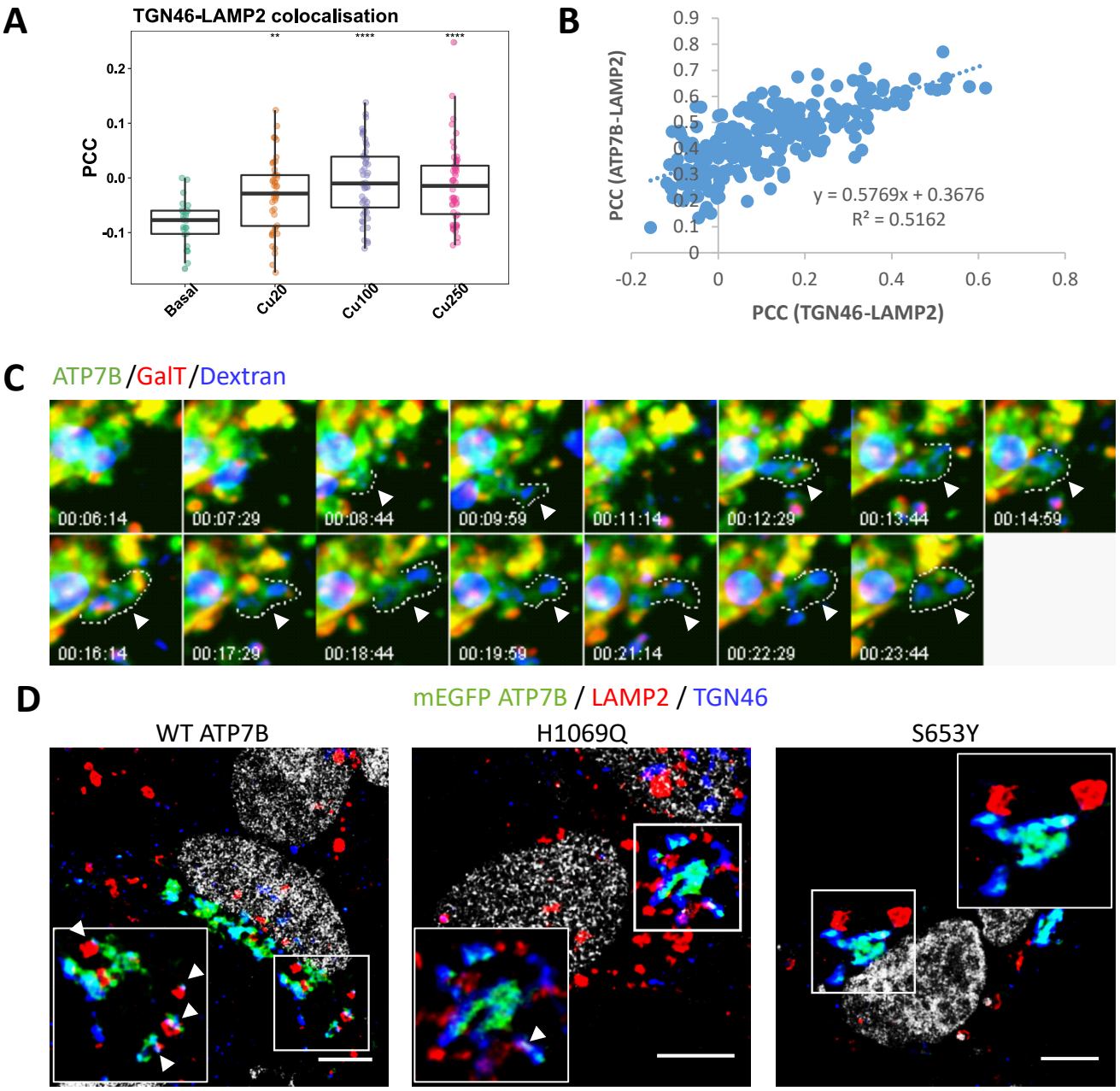
A
TGN46-LAMP2 colocalisation
PCC
0.2
0.1
0.0
-0.1
**
****
****
Basal
Cu20
Cu100
Cu250
B
PCC (ATP7B-LAMP2)
0.9
0.8
0.7
0.6
0.5
0.4
0.3
0.2
0.1
0
y = 0.5769x + 0.3676
R² = 0.5162
-0.2
0
0.2
0.4
0.6
0.8
PCC (TGN46-LAMP2)
C
ATP7B/GalT/Dextran
00:06:14
00:07:29
00:08:44
00:09:59
00:11:14
00:12:29
00:13:44
00:14:59
00:16:14
00:17:29
00:18:44
00:19:59
00:21:14
00:22:29
00:23:44
D
mEGFP ATP7B / LAMP2 / TGN46
WT ATP7B
H1069Q
S653Y

Fig 6

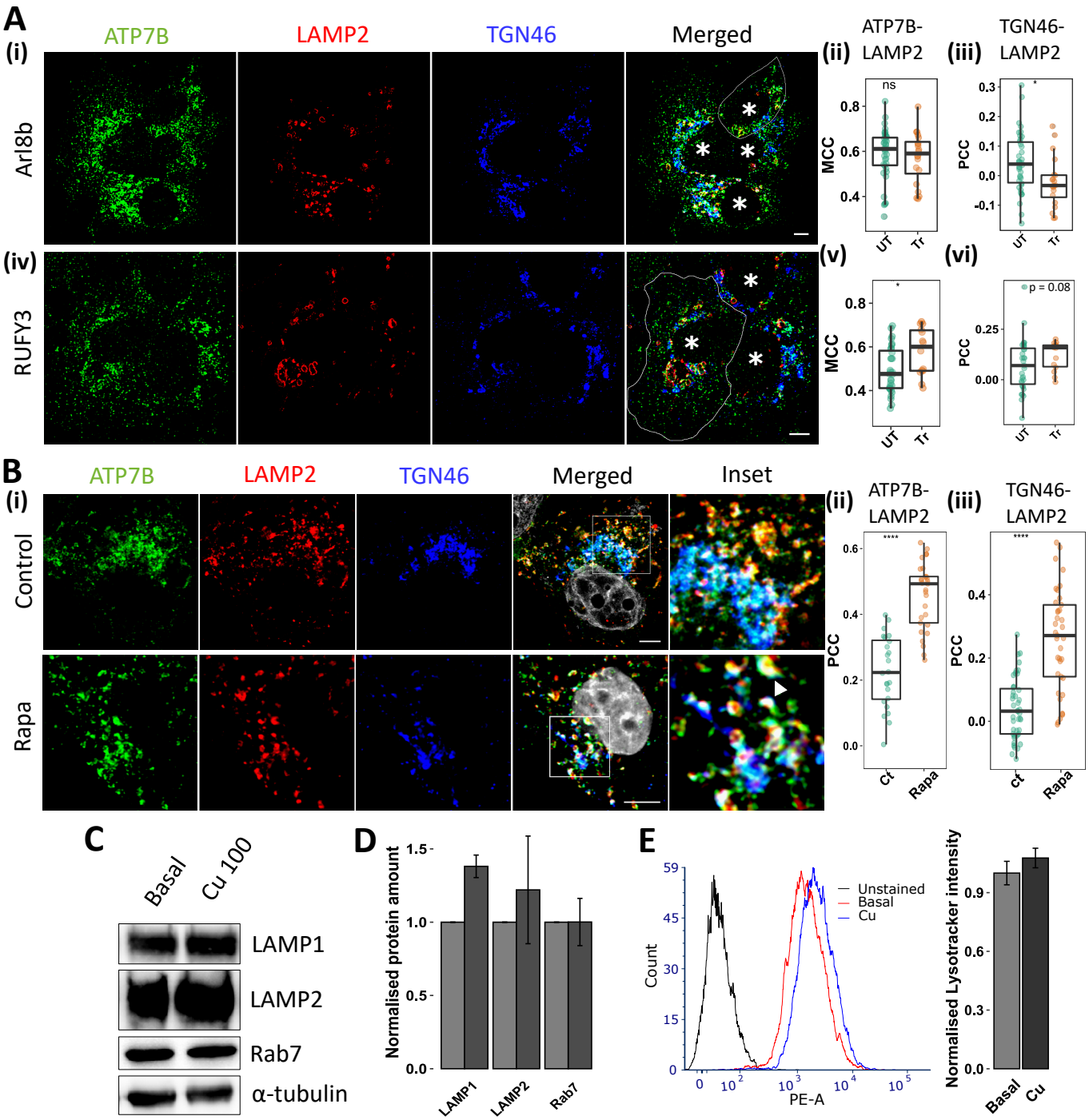
A
(i)
ATP7B
LAMP2
TGN46
Merged
Arl8b
(ii)
ATP7B-LAMP2
(iii)
TGN46-LAMP2
MCC
PCC
ns
UT
Tr
(iv)
RUFY3
(v)
(vi)
p = 0.08
B
(i)
Inset
Control
Rapa
(ii)
(iii)
****
Ct
C
Basal
Cu 100
LAMP1
LAMP2
Rab7
α-tubulin
D
Normalised protein amount
E
Unstained
Basal
Cu
Count
PE-A
Normalised Lysotracker intensity

Fig 7

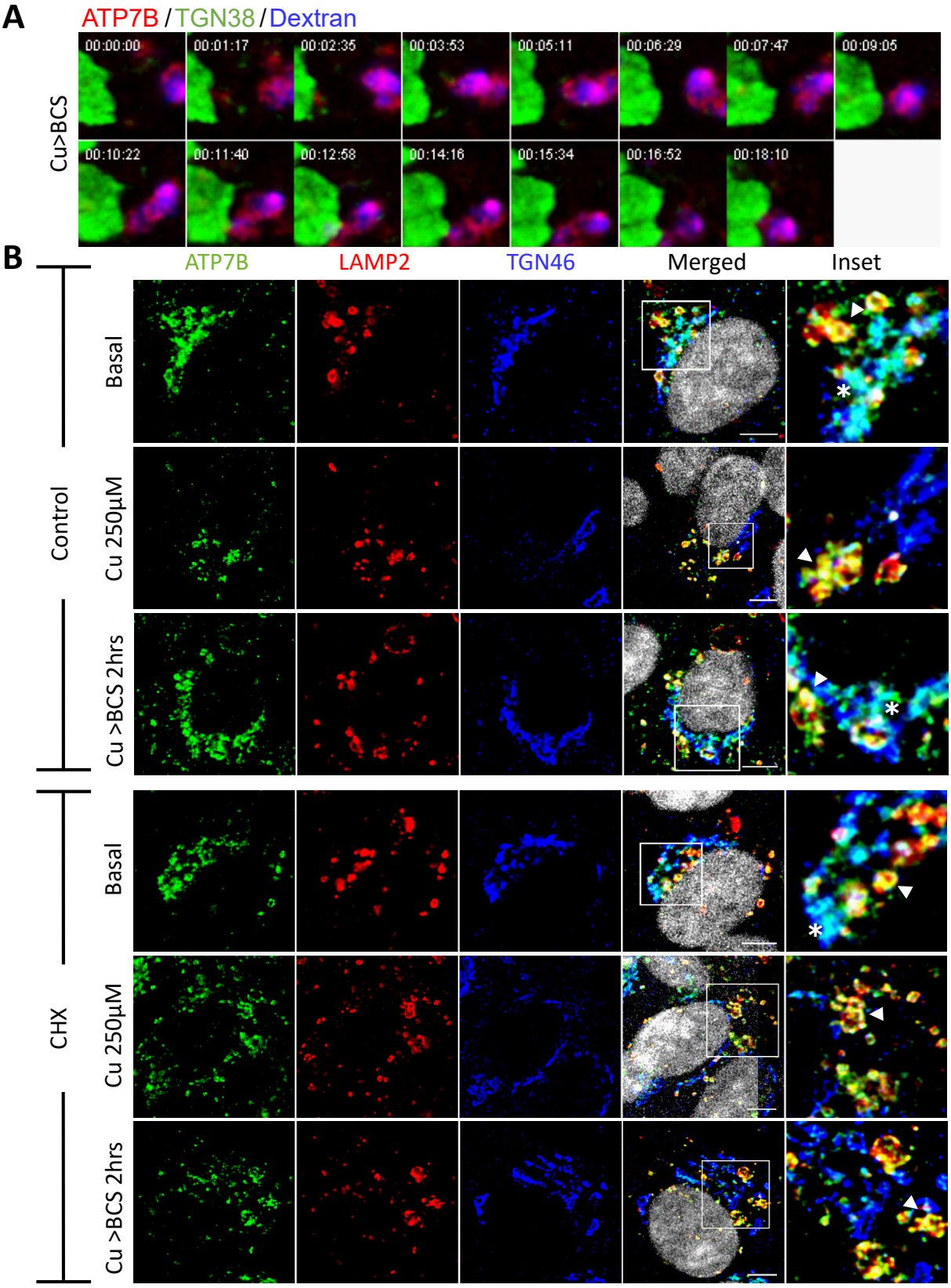
A
ATP7B / TGN38 / Dextran
Cu>BCS
00:00:00
00:01:17
00:02:35
00:03:53
00:05:11
00:06:29
00:07:47
00:09:05
00:10:22
00:11:40
00:12:58
00:14:16
00:15:34
00:16:52
00:18:10
B
ATP7B
LAMP2
TGN46
Merged
Inset
Control
Basal
Cu 250µM
Cu >BCS 2hrs
CHX
Basal
Cu 250µM
Cu >BCS 2hrs

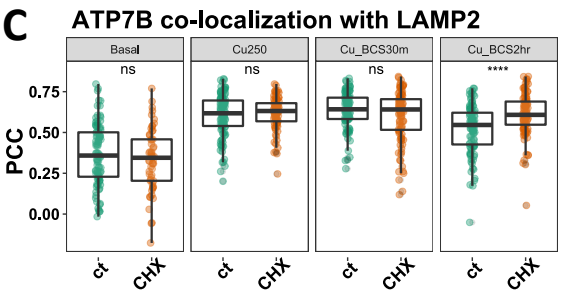
C
ATP7B co-localization with LAMP2
Basal
Cu250
Cu_BCS30m
Cu_BCS2hr
ns
ns
ns
****
PCC
0.75
0.50
0.25
0.00
ct
CHX

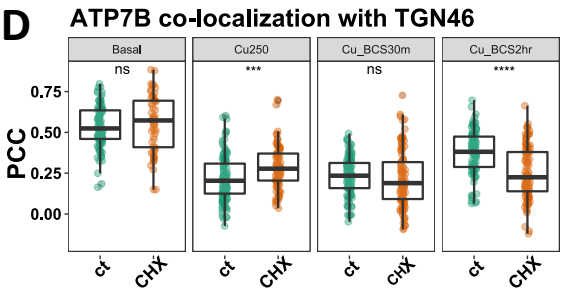
D
ATP7B co-localization with TGN46
Basal
Cu250
Cu_BCS30m
Cu_BCS2hr
ns
***
ns
****
PCC
0.75
0.50
0.25
0.00
ct
CHX

Fig 8

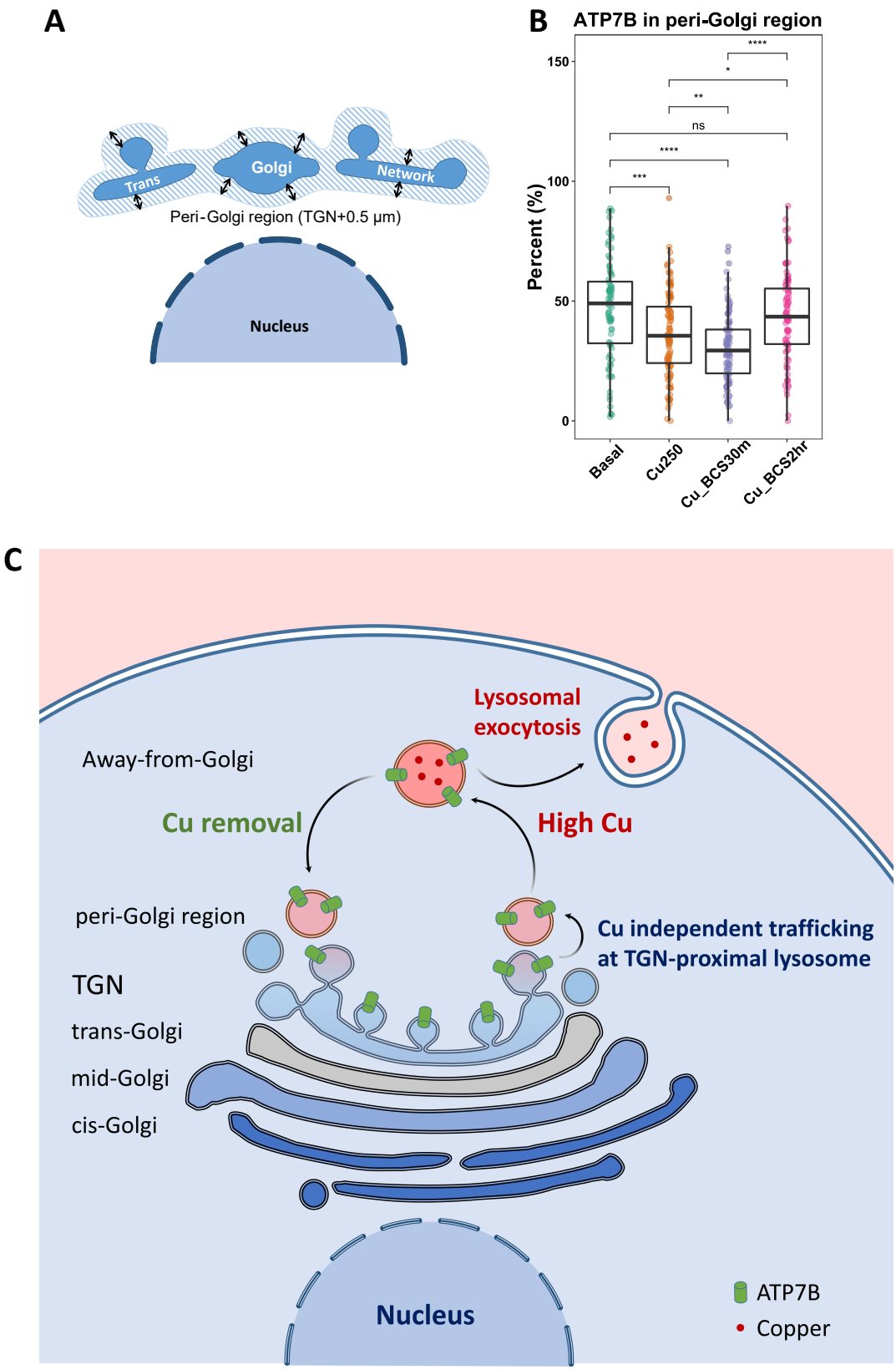
A
Trans
Golgi
Network
Peri-Golgi region (TGN+0.5 μm)
Nucleus
B
ATP7B in peri-Golgi region
Percent (%)
150
100
50
0
****
*
**
ns
****
***
Basal
Cu250
Cu_BCS30m
Cu_BCS2hr
C
Lysosomal exocytosis
Away-from-Golgi
Cu removal
High Cu
peri-Golgi region
Cu independent trafficking at TGN-proximal lysosome
TGN
trans-Golgi
mid-Golgi
cis-Golgi
Nucleus
ATP7B
Copper

Fig S1

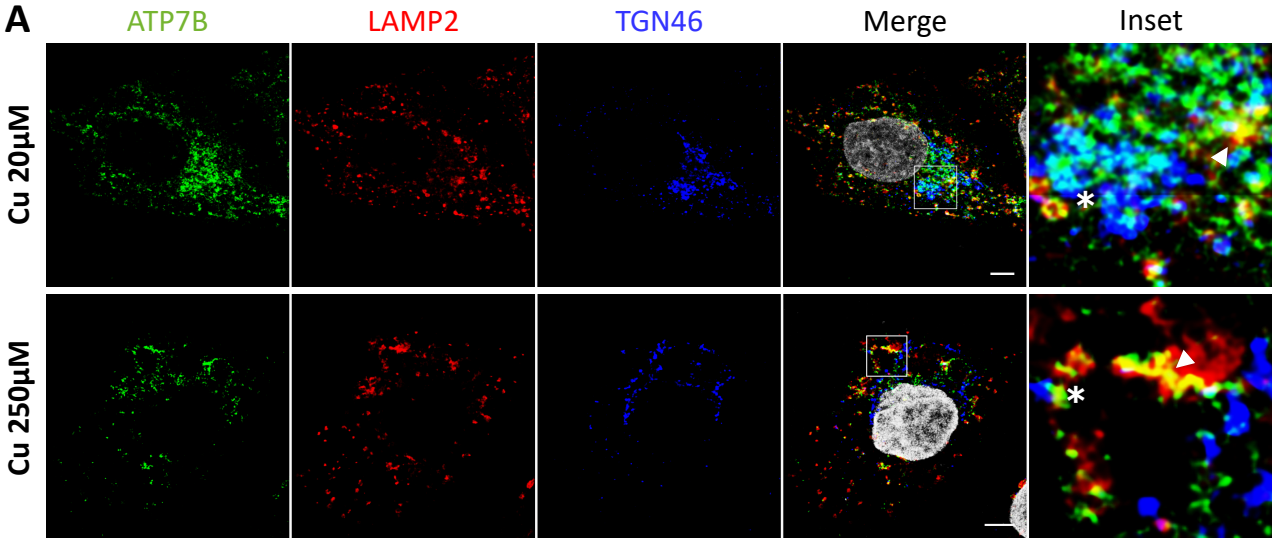
A
ATP7B
LAMP2
TGN46
Merge
Inset
Cu 20µM
Cu 250µM

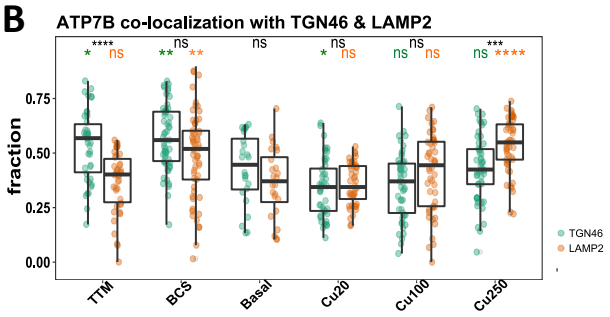
B
ATP7B co-localization with TGN46 & LAMP2
fraction
0.75
0.50
0.25
0.00
TTM
BCS
Basal
Cu20
Cu100
Cu250
TGN46
LAMP2

Fig S2

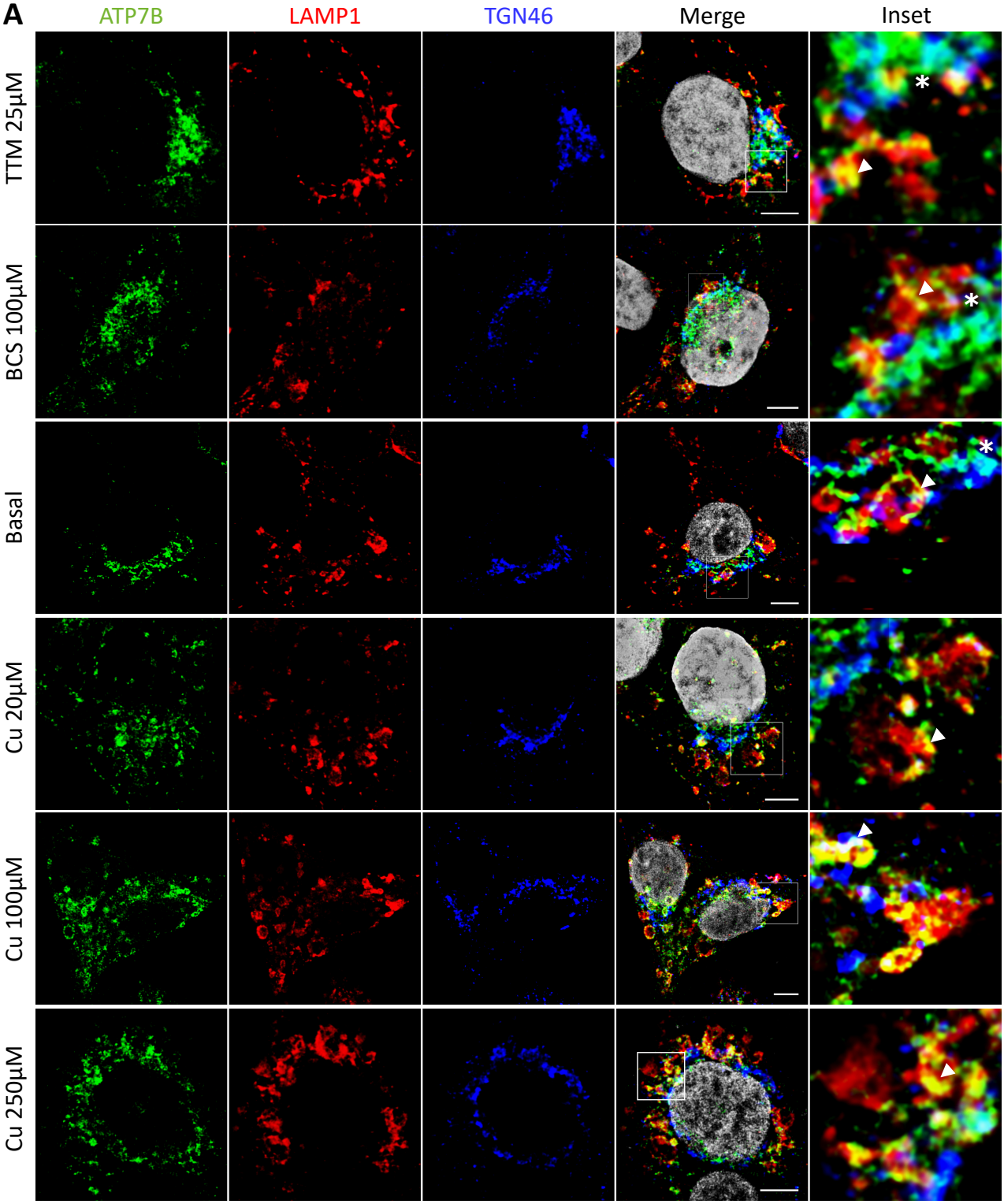
A
ATP7B
LAMP1
TGN46
Merge
Inset
TTM 25µM
BCS 100µM
Basal
Cu 20µM
Cu 100µM
Cu 250µM

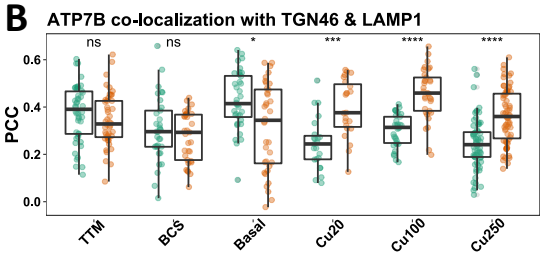
B
ATP7B co-localization with TGN46 & LAMP1
PCC
0.0
0.2
0.4
0.6
ns
ns
*
***
****
****
TTM
BCS
Basal
Cu20
Cu100
Cu250

Fig S3

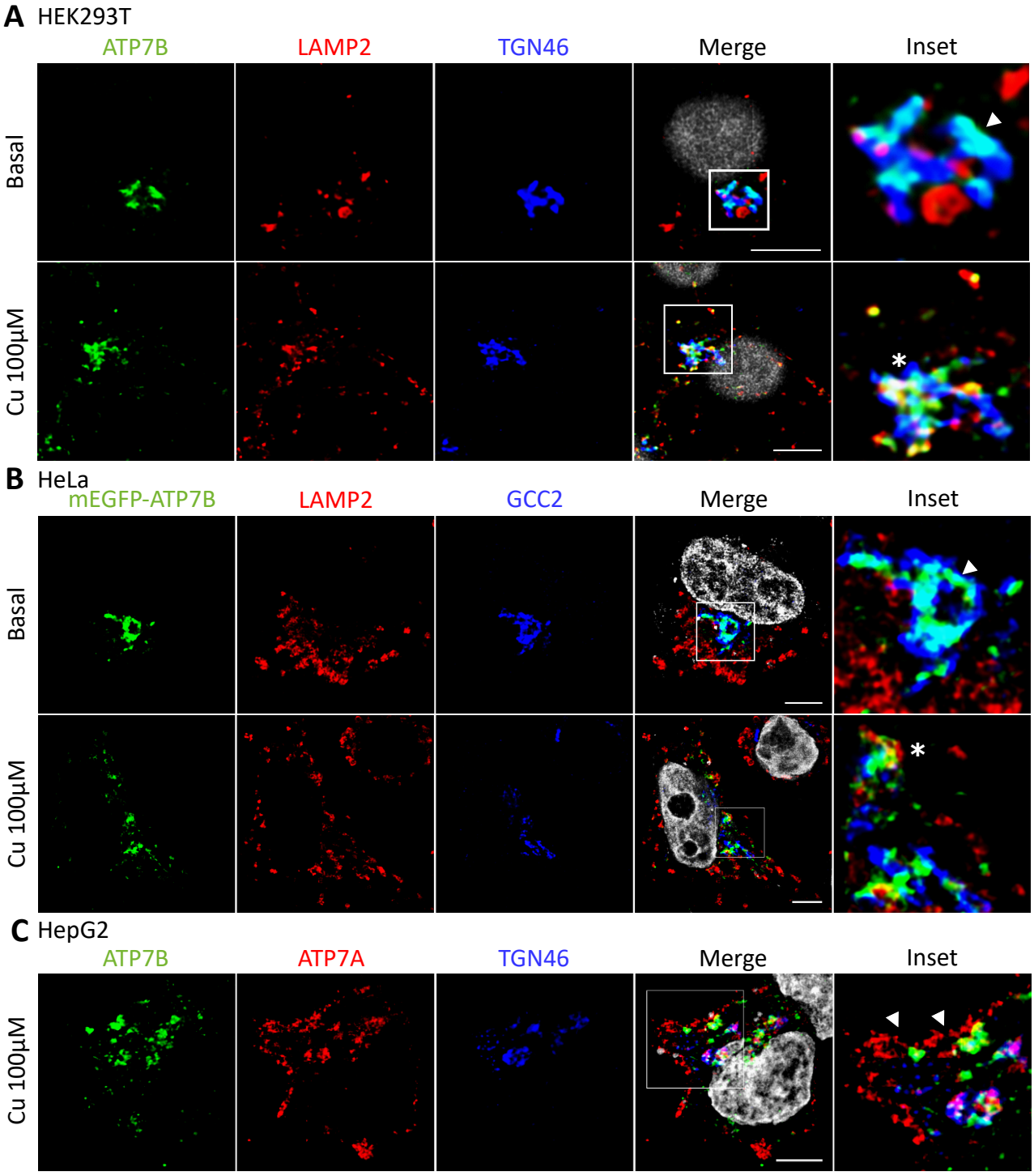
A HEK293T
ATP7B
LAMP2
TGN46
Merge
Inset
Basal
Cu 100µM
B HeLa
mEGFP-ATP7B
LAMP2
GCC2
Merge
Inset
Basal
Cu 100µM
C HepG2
ATP7B
ATP7A
TGN46
Merge
Inset
Cu 100µM

Fig S4

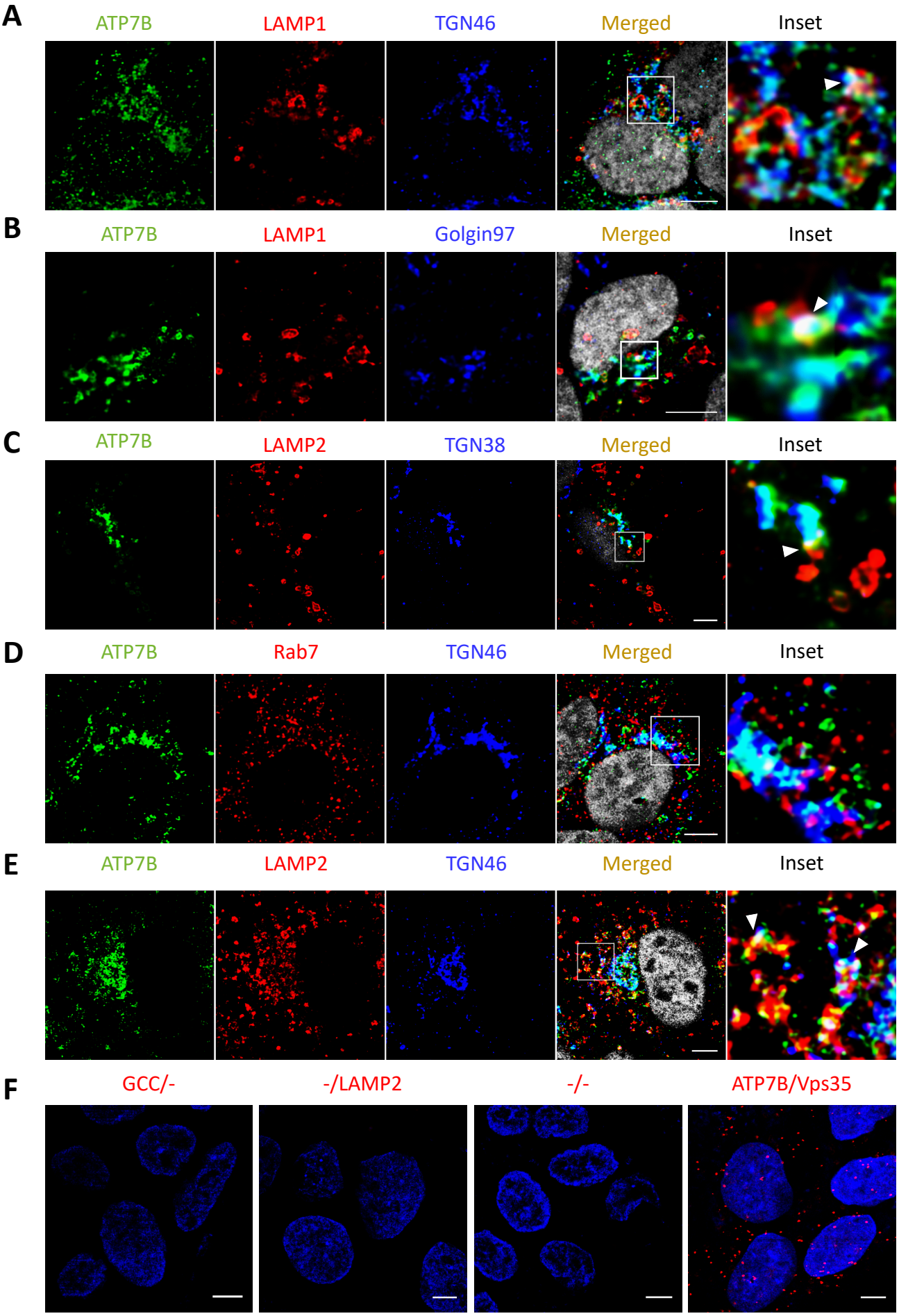
A
ATP7B
LAMP1
TGN46
Merged
Inset
B
ATP7B
LAMP1
Golgin97
Merged
Inset
C
ATP7B
LAMP2
TGN38
Merged
Inset
D
ATP7B
Rab7
TGN46
Merged
Inset
E
ATP7B
LAMP2
TGN46
Merged
Inset
F
GCC/-
-/LAMP2
-/-
ATP7B/Vps35

Fig S5

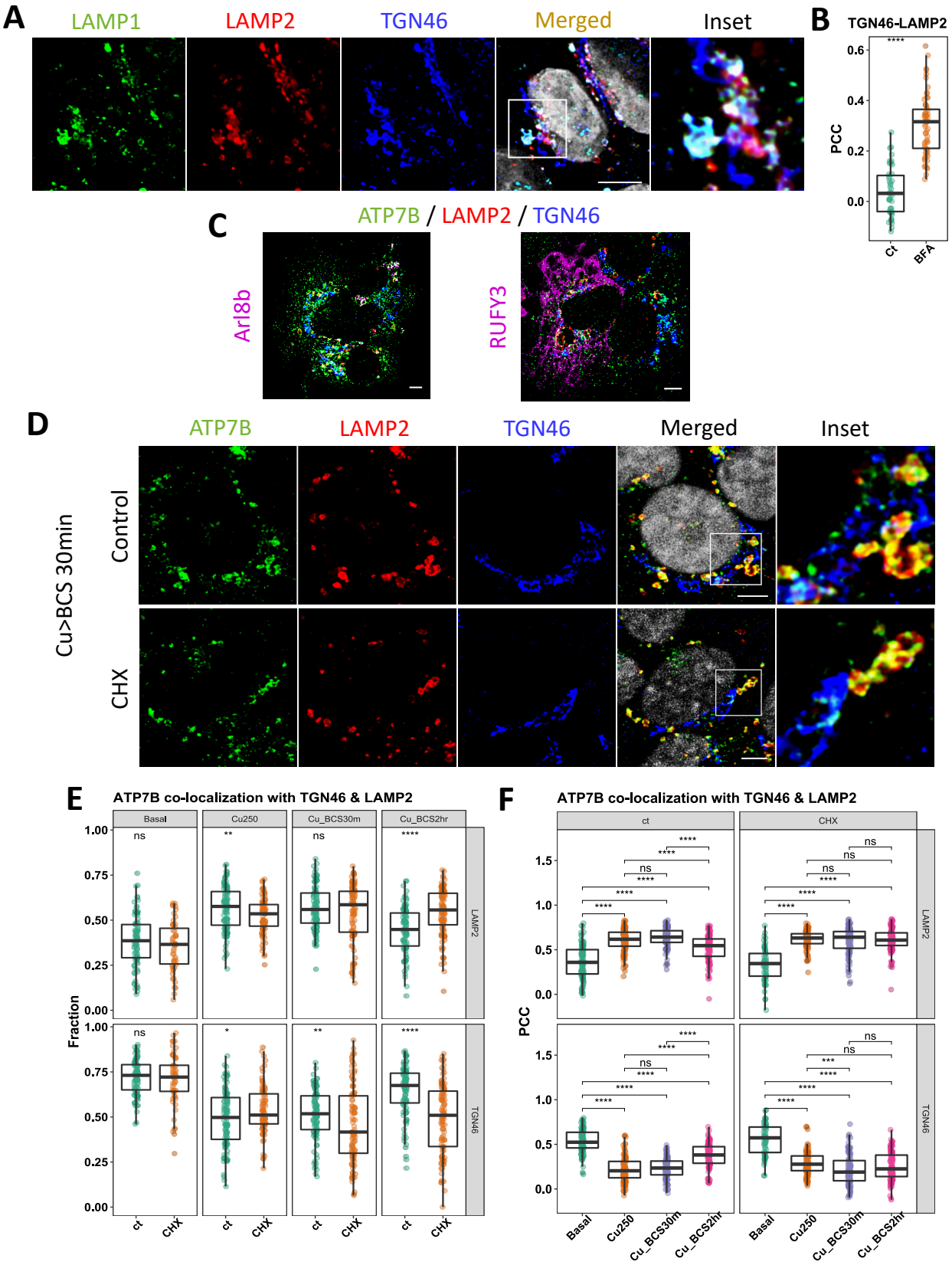
A
LAMP1
LAMP2
TGN46
Merged
Inset
B
TGN46-LAMP2
PCC
ct
BFA
C
ATP7B / LAMP2 / TGN46
Arl8b
RUFY3
D
ATP7B
LAMP2
TGN46
Merged
Inset
Cu>BCS 30min
Control
CHX
E
ATP7B co-localization with TGN46 & LAMP2
Basal
Cu250
Cu_BCS30m
Cu_BCS2hr
LAMP2
TGN46
Fraction
ct
CHX
F
ATP7B co-localization with TGN46 & LAMP2
ct
CHX
PCC
Basal
Cu250
Cu_BCS30m
Cu_BCS2hr